Study and Design of Antennas to be Used in the Vicinity of the Human Body

Fernando José Martins Garcia

Thesis to obtain the Master of Science Degree in

Electrical and Computer Engineering

Supervisor(s): Professor António Manuel Restani Graça Alves Moreira

Examination Committee

Chairperson: Professor José Eduardo Charters Ribeiro da Cunha Sanguino

Supervisor: Professor António Manuel Restani Graça Alves Moreira

Member of the Committee: Professor Paulo Sérgio de Brito André

November 2016

Dedicated to my family, friends and girlfriend

Acknowledgments

I would like to start the acknowledgements by thanking the person that guided me through all this rewarding experience, Professor António Alves Moreira. He was the one that encouraged me to pursue this topic, helped me whenever I needed, and transmitted the knowledge I required in a compelling way. His love for what he does, and his kindness made this process a very pleasant adventure.

Next, I would like to thank Mr. Carlos Brito, the person that led me over the fabrication process of the antennas and took some of his time to explain the whole process for my own enlightenment. He also showed great professionalism and care for my project.

A big thank you to Engineer António Almeida. He was the person that mounted the different scenarios for measuring the antennas, and took some of his own time to perform the measurements. He also showed great professionalism in the way he treated so carefully the procedure and respected my work.

My warmest thank you to a colleague and dear friend of mine, Rodrigo Lourenço, who had had previous contact with patch antennas and the $CST^{TM} MicrowaveStudio$ software, and took some of his personal time to help me throughout my dissertation. He guided me through the complexity of the software, and gave me his knowledge on how to design microstrip patch antennas. His availability and friendship were fundamental to both this project and my academic path.

I would like to thank my family, who unconditionally supported me and allowed for my education at such a prestigious university. To my colleagues and friends, thank you for all the technical discussions and support, that contributed to both my personal and academic growth. I would not be the person that I am today if all of you had not been a part of my life.

Finally, I would like to thank my girlfriend, Jessica Mendes, for all her support and encouragement. She lives in Paris, and despite the distance she made sure I would deliver this dissertation on time and that I put all my effort in it.

Resumo

Hoje em dia, comunicações *wireless* centradas no utilizador são um tópico muito apelativo. Estes sistemas integram antenas na proximidade do corpo humano, e cobrem um leque variado de aplicações, tais como no domínio da saúde, militar ou de entretenimento. De forma a ter um comportamento apropriado, essas antenas têm de ser robustas em relação à influência eletromagnética proveniente do corpo humano. Dito isto, esta dissertação foca a construção de uma antena de dupla banda, com solução *microstrip*, que funciona nas bandas ISM de 2.45 e 5.8 GHz, e que é quase-imune à dessintonia das frequências de operação e à degradação da *performance* da antena quando colocada junto a tecidos do corpo humano. A antena proposta é simulada no software $CST^{TM} MicrowaveStudio$, impressa através de um processo fotolitográfico num substrato $RogersRT/Duroid^{TM} 5880$ e medida, tanto em espaço-livre como junto ao corpo. Em termos de simulação, a antena preenche todos os requisitos estabelecidos a priori para parâmetros fundamentais, tais como o coeficiente de reflexão, as bandas de funcionamento, o padrão da radiação e os valores *SAR*. Em termos de medições, a antena de dupla banda mostra uma grande sincronia com os resultados esperados, e é vista como adequada para comunicações para fora do corpo.

O mesmo procedimento é aplicado a uma antena com banda ultra-larga, e com uma alimentação em *CPW*. Esta é avaliada junto ao corpo humano, em condições semelhantes, com o propósito de alargar o estudo para antenas com diferentes soluções de alimentação e com diferentes frequências de operação. Esta antena é severamente afetada pela influência dos tecidos humanos, quando comparada com a antena em dupla banda. No entanto a antena com banda ultra-larga apresenta o comportamento esperado, e serve como complemento para este estudo.

Palavras-chave: comunicações *wireless* centradas no utilizador, antena com dupla banda, antena com banda ultra-larga, influência eletromagnética do corpo humano, coeficiente de reflexão, modelos de *phantom* simples.

Abstract

Body-centric wireless communications are a hot topic nowadays. These systems employ antennas in the vicinity of the human body, and cover a wide range of applications, such as in the healthcare domain, the military one, or even for entertainment. In order to properly function, the antennas must be robust against the electromagnetic influence of the human body. In light of that, this dissertation focuses on the construction of a microstrip dual-band patch antenna, that works in the ISM bands of 2.45 and 5.8 GHz, and is quasi-immune to frequency detuning and performance degradation, when in presence of human body tissues. The proposed antenna is simulated in $CST^{TM} MicrowaveStudio$, printed photolithographically on $RogersRT/Duroid^{TM} 5880$ and measured, both in free-space and on-body. In terms of simulation, the antenna fulfils the requirements established for the critical parameters, such as return loss, operating bands, radiation pattern and SAR values. In terms of measurements, the dual-band antenna shows a great agreement with the expected results, and is seen suitable for off-body applications.

The same procedure is applied to a CPW-fed UWB-antenna. The latter is also evaluated in the proximity of a human user, on similar conditions, and its purpose is to extend the study to different feeding solutions and antennas with different operating bands. The antenna is seen to be severely affected by the influence of the body tissues, compared to the previous antenna. Nevertheless, the UWB antenna has the expected behaviour, and serves as a complement to the whole case study.

Keywords: body centric wireless communications, dual-band antenna, UWB antenna, human body electromagnetic influence, reflection coefficient, simple phantom models.

Contents

List of Tables

List of Figures

Glossary

BCWC	Body Centric Wireless Communications
CAD	Computer Aided Design
CPW	Coplanar Waveguide
CST	Computer Simulation Technology
FIT	Finite Integration Technique
GCPW	Grounded Coplanar Waveguide
GPS	Global Positioning System
HFSS	High Frequency Structure Simulator
ICNIRP	International Commission on Non-Ionizing Radiation Protection
IEEE	Institute of Electrical and Electronics Engineers
IOT	Internet of Things
ISM	Industrial, Scientific and Medical
IS	International System
ITU	International Telecommunications Union
LOS	Line of Sight
MICS	Medical Implant Communication Service
PCB	Printed Circuit Board
RFID	Radio Frequency Identification
RF	Radio Frequency
SAR	Specific Absorption Rate
UV	Ultra Violet
UWB	Ultra Wide Band
VNA	Vector Network Analyzer
WBAN	Wireless Body Area Network
WLAN	Wireless Local Area Network
WMTS	Wireless Medical Telemetry Services

Chapter 1

Introduction

This chapter presents the background of the main subject of this dissertation, as well as what motivates the author to pursue this topic. The primary goals are established, in order to guide the reader through every single one of them throughout this study. In the end, the organization of this thesis is displayed, along with its content.

1.1 Background and Motivation

The concept of wireless communication goes back to 1864, when James Clerk Maxwell showed the propagation of electromagnetic waves in free space in theoretical and mathematical form. Later proven through an experiment by Heinrich Rudolf Hertz, in 1888, the theory of electromagnetism by Maxwell led several individuals, such as engineers or inventors, to develop radio wave-based systems, which could be used for communicating. Since then, efforts have been made so one could exchange information instantly, over long distances. The world became a smaller place, in which information travels around the globe in a matter of minutes.

The development of new technologies, such as 4G LTE or Wi-Fi, have had its role among society, and led researchers to deepen studies on wireless communications. Combined with technological advances in healthcare and the continuous reduction in size of electronic devices [45] [17], a growing interest in Wireless Body Area Network (WBAN) has been noticed. WBANs englobe a wireless network of wearable computing devices, which may be installed in-body, on-body and off-body [17]. The first category concerns communications from within the human body, through implanted transceivers. On-body communications involve two antennas placed on the surface of the human-body, while the off-body concept relates to a link between only one on-body device and equipment that is not on the human body, but in the surrounding area. Figure 1.1 depicts the gist of body-centric communications.

This dissertation deals with the design of antennas for off-body communication purposes, in the WBAN domain. The other types of communication are out the scope of this work, as the main concern is the study of the interaction between an antenna in the vicinity of the human body and the surrounding equipment.

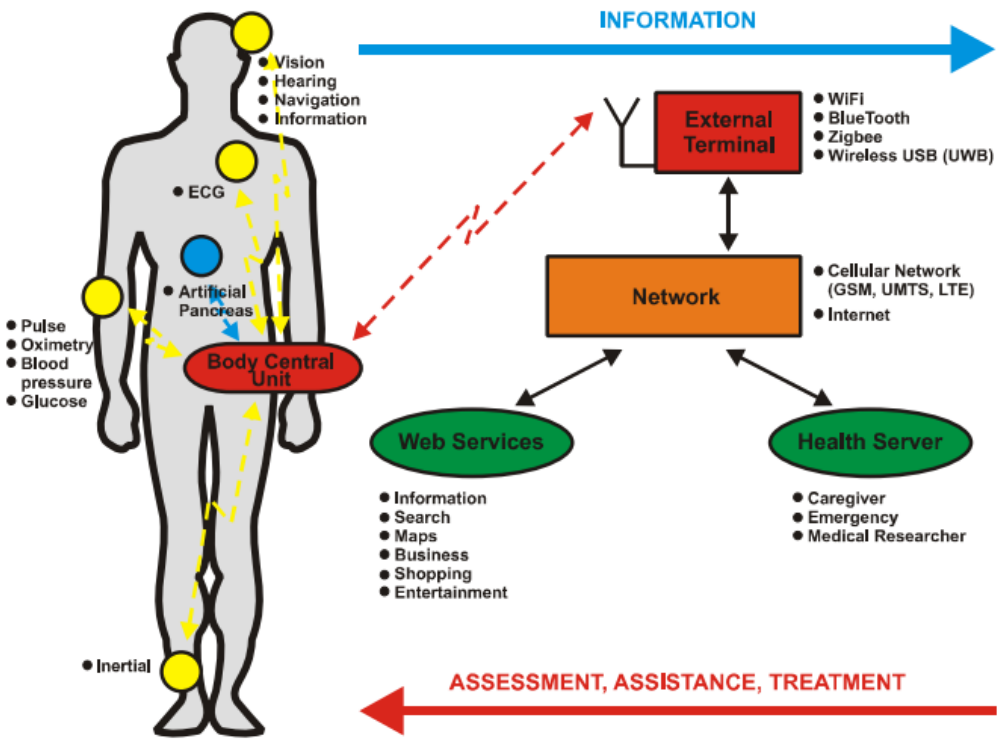

Figure 1.1: Body-centric communications, retrieved from [48].

The main interest in WBANs started in the healthcare domain. For example, wireless medical sensor technologies are of great importance for health monitoring [17] [5], as physiologic data can be extracted from the sensors, which are placed in the human body, and be of use to the doctor at anytime and anywhere. This interest expands to military applications, as one can see in [52], in which body-worn antennas are designed in order to permit communications within patrols, and business, sports, entertainment (where the concept of wearable technology is mostly applied), among others. In order to reach all of these application fields, a standard model was required, so to successfully implement WBAN [33]. Thus, IEEE 802 established a task group, IEEE 802.15.6, which supported an optimized communication standard for low-powered on-body nodes, capable of covering the above-mentioned applications.

Several frequency bands were assigned for WBAN, which may vary according to different countries. Figure 1.2 summarizes some frequency bands allocated for WBAN in different countries. The Medical Implant Communication Service (MICS) band, covered from 402 MHz to 405 MHz, covers implant communication and off-body communications; the Wireless Medical Telemetry Services (WMTS) covers the medical telemetry system and differs in range in Japan and the USA. The 2.45 GHz and 5.8 GHz Industrial, Scientific and Medical (ISM) bands are available worldwide and support high data-rate applications. However, the frequency ranges attributed for ISM (2.4-2.5 GHz and 5.725-5.875 GHz) are subjected to interference, as there are other radio-communication services that operate in the same range, such as the IEEE 802.15.4 (ZigBee), which operates in the range 2.4-2.4835 GHz, or the IEEE 802.15 (Bluetooth), which operates from 2.4 GHz to 2.4835 GHz. Finally, the Ultra Wide Band (UWB), which varies from 3.1 GHz to 10.6 GHz, in both Europe and America, only differing in Japan, from 3.4 GHz to 10.25 GHz. The antennas approached in this thesis are designed to operate in the ISM band

(center frequencies, 2.45 GHz and 5.8 GHz), defined by article 5, footnote 5.150, of the International Telecommunications Union (ITU) Radio Regulations [24], and in the UWB band (frequency range from 3.1 GHz to 10.6 GHz, according to the European UWB radio regulatory and standards, [18]).

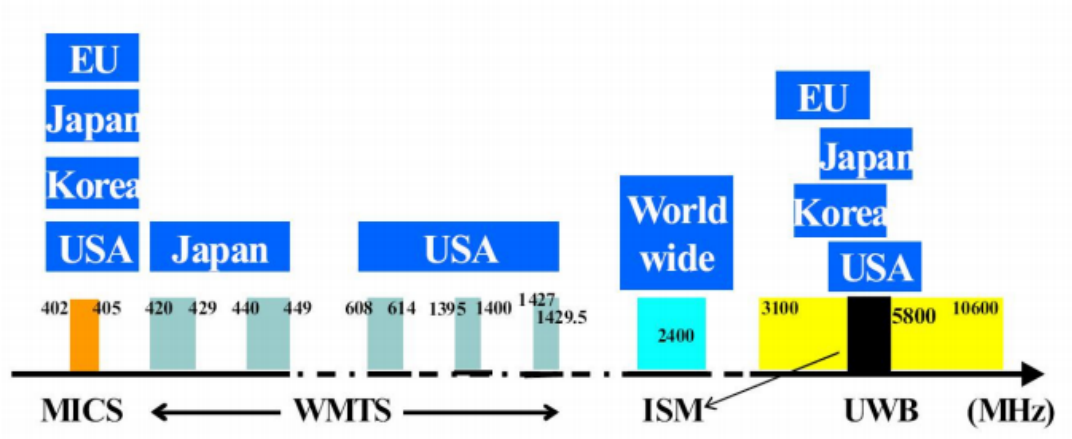

Figure 1.2: Frequency bands for WBAN in different countries, retrieved from [33].

The previously mentioned combination between body-worn devices and miniaturized flexible electronics can be taken advantage of so to allow users to wear the antenna structures, instead of carrying them, which makes the wearable communication systems another interesting topic for research. The design procedure of wearable antennas will further be exploited, but the general idea is to arrange the antenna layout, simulate it, using CST, and optimize it, so it can be built and tested. The process involves:

- Selection and dielectric characterization (electric conductivity, loss tangent, relative permittivity) of the conductive and substrate materials;
- Antenna design (geometry, radiating element, feeding structure);
- Numerical simulation and optimization, using CST;
- Specific Absorption Rate (SAR) calculation;
- Antenna fabrication;
- Antenna measurements (return loss, conclusions on the behaviour of the antennas when put in the proximity of the human body);

1.2 Objectives

The main objective of this dissertation is to study and develop a robust dual-band microstrip patch antenna for body-centric communications, that work in the ISM bands of 2.45 and 5.8 GHz, for off-body applications. The antenna is designed to be compact, easily integrated, immune to detuning and performance degradation, when in the vicinity of the human body. For that, it is inspired on both a

microstrip conventional antenna and the one studied in [55]. A second antenna is also to be developed, an UWB one, in order to complete the study on patch antennas. This antenna comes as a secondary project, to allow the author to compare antennas that function in different operating bands, as well as with distinctive feeding solutions, and is based on the antenna developed in [30].

The main concern throughout this work is the interaction between the proposed antennas and the human body. On that note, the antennas are designed and simulated using the $CST^{TM} MicrowaveStudio$ software, and then fabricated through chemical etching. From the simulation process it is expected to obtain results regarding the critical parameters of the antennas, in order to verify their robustness against the electromagnetic influence of the human body tissues. Such parameters are the return loss, the operating bands, the radiation pattern and the total efficiency of the antenna, which are crucial factors to measure it and evaluate if it fulfils the necessary requirements or not. As for the measurements, it is expected to only evaluate the influence of the human body on the $|S_{11}|$ parameter of the antennas and their operating bands.

Mainly, the dissertation compares the performance of both antennas in different scenarios, such as free-space and on-body. In terms of simulation, the antennas are designed and enhanced using the $ParameterSweep$ and the $Optimizer$ tool from CST. The assessment of the performance of the antennas when put on a human limb is achieved through numerical phantoms. The simulated results are compared with the measured ones, and conclusions are drawn from that.

1.3 Dissertation Organization and Contents

The current dissertation is divided in five chapters. The first one is the present one. Chapter 2 presents the state of the art of antennas that are meant to operate in the vicinity of a human user. For that, the concept of body-centric wireless communications (BCWCs) is exploited, as well as the challenges these systems face and how one can override them. Models of the human body are reviewed, in order to provide a way of testing the performance of the antennas near the human body. Wearable antennas are also introduced. Examples of single-band, dual-band and ultra-wide band (UWB) antennas are reported, so to complement the state of the art of antennas that are carried by the user, and to serve as inspiration for future designs.

Chapter 3 exhibits the whole process of design and optimization of the antennas, in terms of simulation. Several solutions are indicated, that led to the final formats of the outcome antennas. The main parameters, critical for the evaluation of the performance, are simulated.

Chapter 4 compares the simulated results with the measured ones, and assesses the influence of the body tissues on the electromagnetic behaviour of the antennas. For that, their performances are evaluated in different scenarios: free-space, on-body and with the antennas distanced 3 and 7 mm from the user. The measured results on-body are compared to the simulated ones on simple phantom models.

Finally, chapter 5 resumes the whole study and gives feedback on the results obtained. Ideas for future work are also given, focusing on applications for the designed antennas.

Chapter 2

Antennas in the Vicinity of the Human Body

In this chapter, the state of the art of antennas used in the vicinity of the human body is presented, regarding Body Centric Wireless Communications (BCWCs). Models of the human body are introduced, as well as an insight to phantoms. Different technological solutions are explored and highlighted with some examples that one can find in the literature, for the cases of single-band, dual-band and UWB antennas. A comparison among different types of wearable antennas is evaluated, whether they are conventional antennas put in the proximity of the human body or fabric-based. The challenges faced by the latter types of antennas are also taken into account, as well as their main usage.

2.1 Body Centric Wireless Communications

The miniaturization of electronic devices mentioned in chapter 1, section 1.1, led to the study and development of numerous devices and systems that can nowadays be carried by the user, or even be attached to the body. Thus, wearable devices and on-body equipment became interesting topics, for different application fields. As an example for on-body devices, a radio frequency identification (RFID) antenna detects urination for adults, in [28], providing them a comfortable healthcare environment and better quality of medical support. In the military domain, wearable devices can be used in order to offer support to soldiers, whether to provide communications or to monitor their vital signals in combat conditions. In light of this, BCWCs started being heavily investigated.

For BCWCs, the design of the antennas must be carefully chosen, as one of the major challenges for on-body antennas in the WBAN domain is the interaction of the antenna with the human body [45][28]. As it is considered a lossy medium, with high loss and permittivity, the antennas should be compact, small and robust to detuning and performance degradation. The type of antenna must also be taken into account, as not all are adjustable to the body dynamics. Moreover, the surrounding area must be given consideration, as it can affect directly the link between the on-body device and the source or terminal.

Another challenge faced by BCWCs is the shadowing phenomena. Not only some parts of human

body may obstruct the line of sight (LOS) between the transmitter and the receiver, the antenna itself may suffer from misalignment or pattern distortion [48]. Also, reflections often occur, derived from natural movements, such as the swing of the arms or legs [11] [25]. Therefore, all of the mentioned characteristics must condition the body-antennas, and can be evaluated through numerical analysis and by studying the electromagnetic fields around the antenna, as well as its radiation signature. The measurement setup may be accomplished by using phantoms, as they serve as a good model of the human body, by simulating its main biological characteristics, both numerically and physically.

Phantoms have been broadly used in studies that concern the interaction of electromagnetic fields and the human body. They can be simple or more complex ones, depending on the degree of precision needed for the project at hand, and are fully detailed in the next section.

2.2 Modeling of the Human Body

To optimally design an antenna that is meant to operate in the vicinity of the human body, the interaction between the human tissues and the electromagnetic (EM) waves must be accurately analysed. As previously mentioned, the antenna radiation pattern and matching can be severely affected, performance that depends on the frequency range and the spatial orientation of the transmitter to the receiver [25]. Numerical models of the environment that surrounds the antenna can be simulated, although they translate an ideal situation where several interferences are not accounted for (such as mechanical ones [22] [47]). Thus, the best way to evaluate the behaviour of an antenna in the proximity of the human body is to resort to an actual human user [42]. However, the antennas must obey to certain requisites, one of them being the Specific Absorption Rate (SAR) in the human body. This parameter measures the power absorbed by the human body (when exposed to electromagnetic waves) per mass of tissue, and can not surpass a stipulated value. Hence, and as the SAR value can only be defined in a simulation software environment, before the antenna is submitted to experimental tests, numerical and physical human body models, denominated *phantoms*, started being used for a more profound simulation and investigation of the behaviour of the antennas. Otherwise, it would not be ethical to subject human lives to such possible harmful scenario, in which the antennas may exceed the maximum SAR value and subject the human body to a dangerous amount of radiation absorption.

2.2.1 Phantoms

A phantom serves to mimic human tissue, so it should comprise detailed information of the human body (or of just specific areas, like the head or an upper arm). From a realistic anatomic shape, to the dielectric features of the several human tissues, the phantom presents itself as an efficient tool to characterize BCWCs.

The phantoms can be accomplished experimentally or numerically [64]. The first ones require real physical structures, thus limiting the mobility needed to evaluate, in terms of body shape. Compared to numerical models, are also more expensive, as they have to be physically constructed with gel materials

that possess the dielectric properties of the human tissues [23] [11] [64]. The numerical body phantoms simulate the physiologic data of the human body and are based on phantoms embedded in electromagnetic codes. For the case of wearable antennas, numerical phantoms are more desirable for simulating the human tissues [64].

In the literature there is presented a broad collection of papers that evaluate the behaviour of on-body antennas by resorting to phantoms. These models can be simple ones, whether homogeneous (in which only a single dielectric material is used) or heterogeneous (which comprise several human tissues, mainly skin, fat, muscle and bone), or more complex, such as voxel models [7] [63] [25]. In [30], simple multi-layered and frequency-dependent structures of the human body were taken into account, which are shown in Figure 2.1. The models, with rectangular and elliptical shapes, consider the dispersion of the tissues employed (skin, fat, muscle and bone) throughout the UWB operating bandwidth. The effect of the elliptical and flat model on the antenna impedance bandwidth are very similar and the simulated results predict well the behaviour of the antenna, in the vicinity of the human body. In fact, the measured results show that the simplified elliptical model employed is accurate enough to simulate the input reflection coefficient of the antenna in the proximity of the human body.

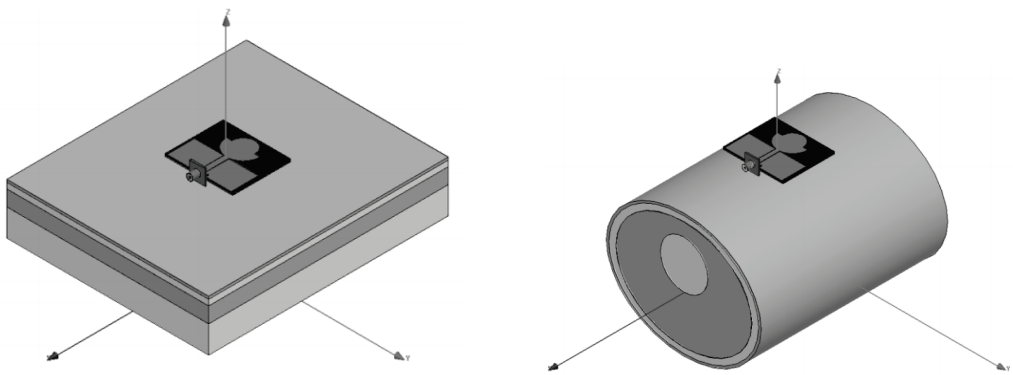

(a) Flat model. (b) Elliptical model.

Figure 2.1: Simplified models used for simulation, retrieved from [30].

In [11], the designed antenna is tested in the vicinity of the human body, firstly using a physical single-layer and frequency-independent phantom which models a human arm, and secondly using a numerical high-resolution whole-body voxel model, so to characterize it for on-body propagation. The simple model uses a dielectric with a permitivitty equivalent to two thirds of the one of a human muscle (shown in Figures 2.2(a) and 2.2(b)), and the numerical model uses a whole-body human model from the Virtual Family [16], with high-fidelity anatomical detail (the used model is Duke, pictured in Figure 2.2(c), which is a three-dimensional model of a thirty-four year old male adult, that heights hundred and seventy four centimetres and weighs seventy kilograms, with high-resolution magnetic resonance imaging data segments that yield up to more than eighty different tissues and organs [16]). The experimental and numerical results with both phantoms showed that the body does not affect considerably the antenna input matching, thus exhibiting that the physical phantom represented by an homogeneous model with two-thirds the permittivity of the muscle was enough to successfully measure the reflection coefficient and the radiation patterns of the designed compact planar UWB monopole antenna. Furthermore, the

voxel model delivers an analysis of the electromagnetic field propagation around the body, in order to evaluate configurations for achievable wireless radio links within different parts of the human body.

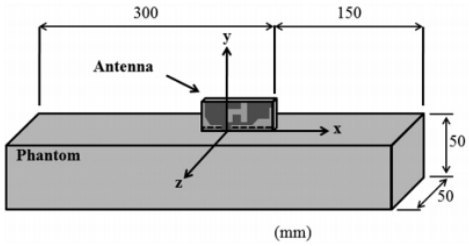

(a) Antenna on the two-thirds muscle-equivalent phantom.

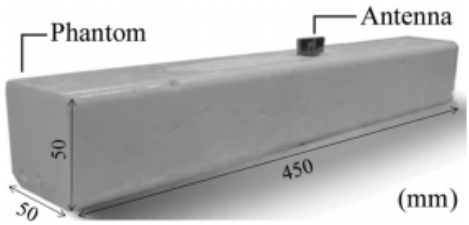

(b) Antenna prototype mounted on the two-thirds muscle-equivalent phantom.

(c) Duke Model, retrieved from [16].

Figure 2.2: Homogeneous phantom, with a permittivity equivalent to two-thirds of the one of a human muscle, retrieved from [11], and a whole-body voxel model from the Virtual Family.

The influence of the human body on the performance of a mobile terminal, and the influence of electromagnetic waves on the human body are interactions that need a careful and thorough evaluation. To do so, physical phantoms are to fulfil several requirements, such as realizing electric constants for a wide frequency range or being low cost [23], and that they can take different shapes according to their intention [64]. Flat models are usually employed to study a simple solution, where energy is radiated from a simple source, such as a small dipole antenna. Spherical models are associated with the investigation of electromagnetic effects in the human head. Cylindrical/elliptical models usually incarnate human limbs, such as arms or legs, in order to evaluate the influence of a whole-body presence on a wireless radio communication. More complicated models can also be fabricated if more accuracy is indispensable, such as the ones explored in [23]. A real-shaped upper-half body phantom is reproduced to inspect the characteristics of the antenna, such as the internal SAR distribution or the influence of the

electromagnetic waves on the radiation patterns. Additionally, the combination of simple models, such as cylindrical and elliptical, conceive a two-layer abdomen phantom that is used to model the abdomen of pregnant women.

On the other hand, microwave [42] and medical [64] imaging techniques have been extensively explored, as the former can be used as a tool to diagnose abnormalities, such as cancerous cells, and the latter as magnetic resonance imaging. Combined with modern softwares, cutting-edge realistic partial and whole-body models with high-resolution have been developed to represent humans of different physiques. These models can be used for more accurate tests than the ones provided by simpler models, as they provide better results on the measurements of electromagnetic fields [64]. These complex models are given preference for distinctive on-body scenarios, with various body postures, or to evaluate the arrangement of on-body mobile terminals linked to one another. However, these phantoms greatly increase computational time when compared to simplified geometries. The choice between simple models (with lower resolution) and high-resolution realistic body models arises from the compromise between the amount of time needed, the accuracy pretended and the available resources that one has at disposal.

2.3 Antennas Operating in the Vicinity of the Human Body

As described in section 2.2, the human body affects tremendously the characteristics of an antenna that is placed in its vicinity, so an understanding of this influence must be carried out so to provide proper communication systems for WBAN applications. Many studies have been conducted in order to evaluate the influence of the human body on antennas, and mainly shown a reduction in the antenna efficiency, due to electromagnetic absorption in human tissues, as well as deformations in the radiation patterns. For example, in [57] a coplanar-fed antenna was designed to operate at 2.45 GHz (ISM band) and close to the human body. The simulation, conducted with a flat and elliptical models of the human arm, shows a detuning of the antenna in the direction of low frequencies, when compared to the results obtained in free space. A decrease in the magnitude of the $|S_{11}|$ parameter is due to the absorption of energy by the human body models. The radiation patterns are also affected, as the lobe directed towards the human tissues is nearly absorbed, due to the high relative dielectric permittivity of the tissues. Nevertheless, the antenna covers the ISM band (at 2.45 GHZ) and is suitable for off-body connections. As another example, in [51], a dual-band textile antenna is studied in the proximity of the human body. The results are simulated and compared with a phantom flat model of the human body. The textile antenna was used in different parts of the body (back, torso and forearm), and the results showed a small antenna detuning in the lower frequencies, but good results for the higher ones, in terms of the -10 dB criteria. The antenna efficiency was evaluated as well, by being determined through full 3D radiation patterns by using a monopole as reference. The results showed that the phantom has a substantial impact, reducing the efficiency by forty percent in the upper bands and ninety percent in the lower band.

In section 2.1, the recent miniaturization of wireless devices has been seen as the main responsible for the rising utilization of wearable antennas. These are translated into conventional antennas, such as

planar dipoles, monopoles or microstrip patches; fabric-based flexible antennas, which employ textiles in the antenna segment [50] [6] [65], and antennas on accessory pieces like buttons or belts [62] [61] [69] [66]. Fabric-based antennas require knowledge on the electromagnetic properties of the textile material, such as permittivity, and loss tangent. These textiles are highly attractive, since the materials they employ have great features, such as excellent radio-frequency (RF) performance, durability, and flexibility. However, one major challenge faced by these types of antennas is the uncertain form of the garment; the performance of the antenna might be degraded when suffering from deformations on the ideal shape, such as bending or crumpling. Other factors must also be taken into account, such as the possibility of textiles getting dirty, or of absorbing humidity. The roughness of the textile can also be seen as a drawback, as the increased surface resistivity reduces the antenna efficiency. The several additional aspects that must be considered when designing an accessory or textiles antennas makes them not as much attractive as conventional antennas, and are out of the scope of this dissertation. The general low cost and simple fabrication of conventional antennas makes them a highly pursued topic, and will be further scrutinized in the following subsections, for the specific cases of single-band, dual-band and UWB antennas, so to function in the proximity of a human limb or whole body.

2.3.1 Single-band Antennas

In chapter 1, section 1.1, the ISM bands (2.45 and 5.8 GHz) were introduced as universal bands that support high data-rate applications, such as radio frequency for industrial, scientific and medical purposes, as well as for telecommunication services, such as wireless local area networks (WLANs), Bluetooth or ZigBee. However, it was also observed that the frequent use of these bands can result in electromagnetic interference among the devices that make use of them, and lead to subsequent radio communication disruption. Communication equipment were afterwards limited to certain bands of frequency and designed in order to tolerate any interference generated by ISM applications. On that note, a simple narrow-band coplanar-fed single-band antenna that works in the 2.45 GHz ISM band was introduced and developed in [58], which is shown in Figure 2.3.

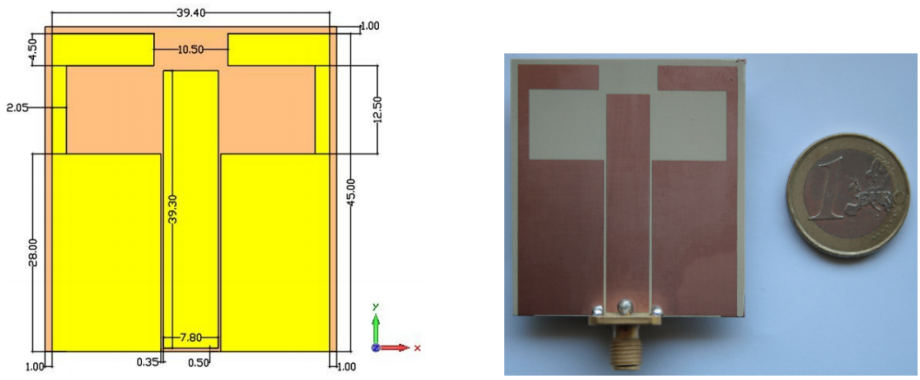

(a) Geometry and design parameters (measures in mm).

(b) Photograph.

Figure 2.3: Coplanar-fed single-band antenna.

The geometry of the proposed antenna is based in [8], and is meant to operate in the vicinity of the

human body. The coplanar waveguide (CPW) solution was kept in order to allow for an easy integration with active devices and because a feed of CPW-type reduces the unwanted coupling in the feed line. The pretended goals for the final product were to have an antenna that was compact, insensitive to detuning (induced by the proximity to the human body), with a SAR below the established limits, even when subjected to deformations, such as bending. In order to achieve the mentioned objectives, the antenna in [8] suffered some changes: the substrate was increased in 1 mm beyond the metal layer, so to increase mechanic stability; the substrate material was changed to $RO3003^{TM}$ (relative permittivity $\varepsilon_{r,@2.45GHz} = 3.0035 \pm 0.04$ and loss tangent $tan\delta_{@2.45GHz} = 0.0006$), as it allows for a good RF performance; the ground plane was designed in order to lengthen higher than $\lambda/4$, so to reduce possible return currents to the cable. Finally, and after analysing the current distribution along the patch, an opening was made above the ground plane, making the antenna perform as an aggregate of two dipoles, as can be seen in Figure 2.4.

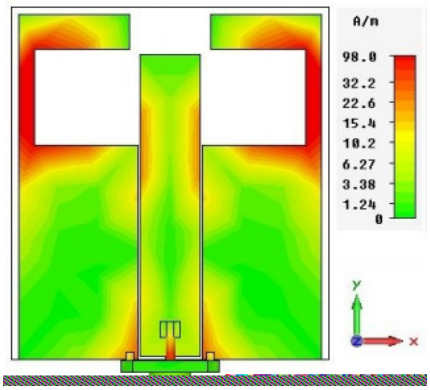

Figure 2.4: Simulated current distribution at 2.45 GHz (in CST).

The T-shaped patch antenna with a 50 Ω coplanar feed line was simulated with the software $CST^{TM} MicrowaveStudio$ in free-space and within 6 mm of the simplified models of the human body outlined in subsection 2.2.1 (see Figure 2.5).

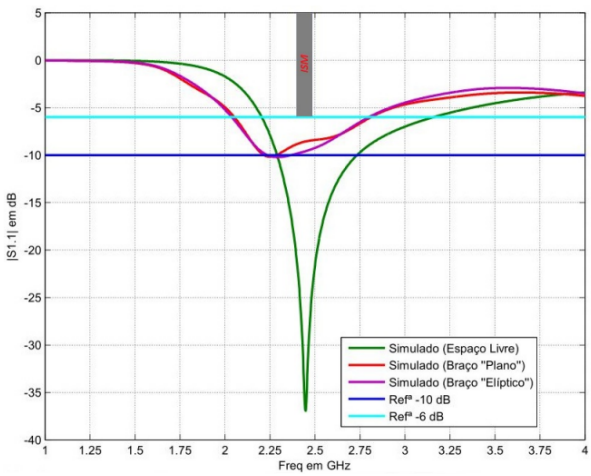

Figure 2.5: Input antenna reflection coefficient parameter, $|S_{11}|_{dB}$, simulated in free-space (in green) and in presence of elliptical (in purple) and flat (in red) models of a human arm.

The considerable effect in the behaviour of the antenna when in presence of the models of the

human body, in both antenna resonance and the antenna reflection coefficient magnitude led the author to pursue another criteria. Until now, the convention used is that an antenna is considered adapted to a certain frequency band when the reflected power is equal or less than ten percent of the incident power (which is translated into $|S_{11}|_{dB} \leq 10dB$). Another criteria, commonly accepted when dealing with antennas employed in mobile terminals [6], consists in considering that the antenna is adapted to the projected frequency band when the reflected power is equal or less than twenty-five percent of the incident power (which is translated into $|S_{11}|_{dB} \leq 6dB$). The latter was applied by the author, and he was able to accurately predict the resonance frequency, despite the slight detuning and considerable reduction in magnitude of the $|S_{11}|$ parameter.

After the simulations, the behaviour of the antenna was evaluated in laboratory, in both free-space and next to the human body situations. Figure 2.6 shows the two scenarios. Also, to study the effect of the human body on the performance of the antenna, two other experiments were conducted: the first one, in which the antenna is tested in the same conditions as in Figure 2.6(b), but with the user wearing a military jacket; in the second one, the effect of the rain was taken into account, and was achieved by spraying the military jacket on the area where the antenna resides. Figure 2.7 compares the results in all the appraised cases.

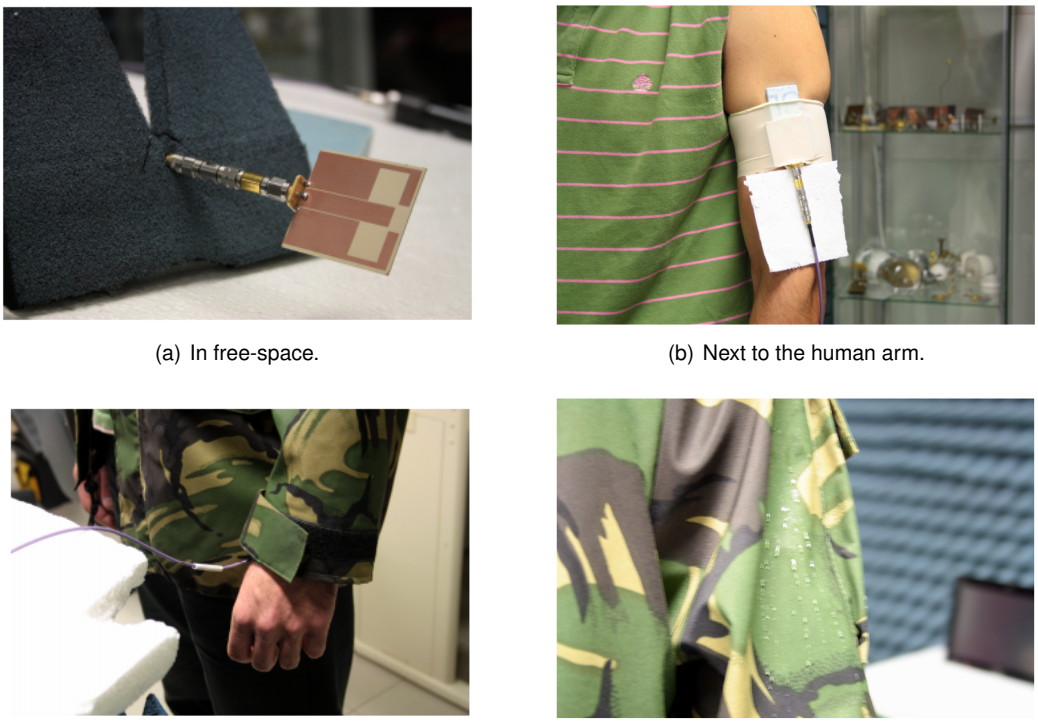

(a) In free-space.

(b) Next to the human arm.

(c) With military jacket.

(d) Water-sprayed military jacket.

Figure 2.6: CPW single-band antenna measurements in laboratory.

It can be seen that the reflection coefficient parameter does not appreciably differ from one scenario to the other, when the antenna is put next to the human body, concluding that in this case the simplified models employed for simulation purposes are an accurate tool for predicting the performance of the designed antenna. However, the outcome is only valid if a reflection up to twenty-five percent of the

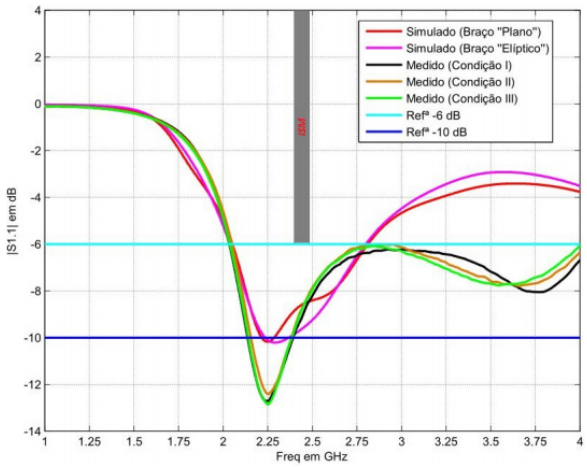

(a) Simulated models of the human arm and wearable cases.

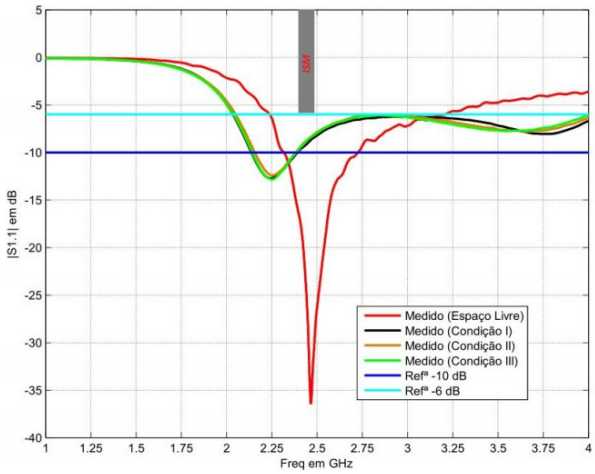

(b) Comparison between the antenna measured in free-space and in the wearable cases.

Figure 2.7: $|S_{11}|$ parameter measured for all cases.

incident power can be backed up.

The measurements were concluded with the calculation of the SAR parameter. In both scenarios the SAR parameter was determined to be below the maximum values allowed (recommended localized SAR value for antennas in human limbs is $4W.Kg^{-1}$ for an averaging mass of 10 grams of contiguous tissue [20]). The obtained results can be consulted in Table 2.1.

2.3.2 Dual-band Antennas

The noticeable rapid growth in WLAN applications not only has demanded higher data rates, but also that single devices operate at more than one frequency band. Antennas that are compact and can be easily integrated into communication systems, combined with multi-functionality (whether they are simply transmitting and/or receiving data, employing redundancy or duplex modes, or functioning as access points so to transmit wireless signal around them), makes antennas with two or more resonance frequencies an alluring subject. Thence, a compact CPW-fed dual-band transparent antenna is designed and developed in [55]. The antenna operates at two distinguished frequency bands: at 2.45 GHz, for

Scenario	Model	Bandwidth [in percentage]	Radiation Efficiency [in percentage]	Total Efficiency [in percentage]	SAR [in $W.kg^{-1}$]
CST Microwave Studio	Free-space	17.53	99.77	98.13	-
	Human arm (elliptical)	31.4	18.05	16.06	1.515
	Human arm (flat)	31.69	15.65	13.47	1.420
Laboratory	Free-space	16.24	95.00	95.00	-

Table 2.1: Summarized results of the research presented in [58].

WLAN access point applications, and at 5.8 GHz, for WLAN point-to-point purposes. The transparency of the antenna comes from a different approach: the author of this antenna used a conductive silver coated film (AgHT-4) as the main material. There has been a growing interest in these type of material, as its main advantages lie in features such as very low thickness, lightweight and high transparency percentage (ninety percent for AgHT-4) [38] [26].

The main objective of this research is to create a transparent antenna that can be integrated into glass (for example, the window glass of a building), in order to function as an access point and provide wireless signal to the surrounding area. In Figure 2.8 the proposed antenna is illustrated. The AgHT-4 thin film includes the silver coated polyester (as the conductive layer) and polyethylene terephthalate (PET) as the substrate. As can be seen, and due to the main purpose of this study, the antenna was integrated on a 1.9 mm thick glass, composing an antenna with an overall size of $60 \times 60 \times 2.075mm^3$.

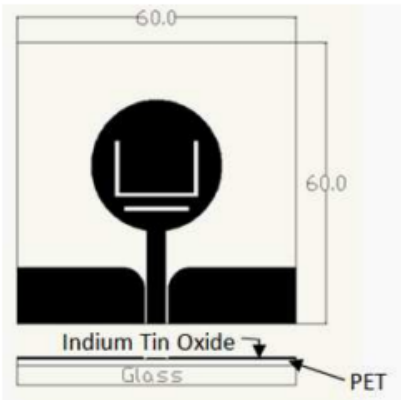

Figure 2.8: Geometry of the CPW-fed dual-band transparent antenna

The author started to evaluate the performance of the designed antenna on the Computer Simulation Technology (CST^{TM}) software. The final dual-band antenna produced, which is composed by the ground plane and a circular radiating element, and fed by a 50 Ω coplanar feed line, was firstly simulated as a simple antenna with no slots (Figure 2.9(a)). It can be seen in Figure 2.10 that the antenna does not resonate at any frequency. Thus, an U-slot was introduced (Figure 2.9(b)). This technique is commonly used so to reduce the size of antennas at a fixed frequency. In Figures 2.9(b) and 2.10 the proper insertion of an U-shaped slot produces a resonance frequency at the desired 2.45 GHz. Moreover, with the insertion of a well-positioned line-slot, a second resonance frequency was achieved, at 5.8 GHz,

without affecting the lower frequency band.

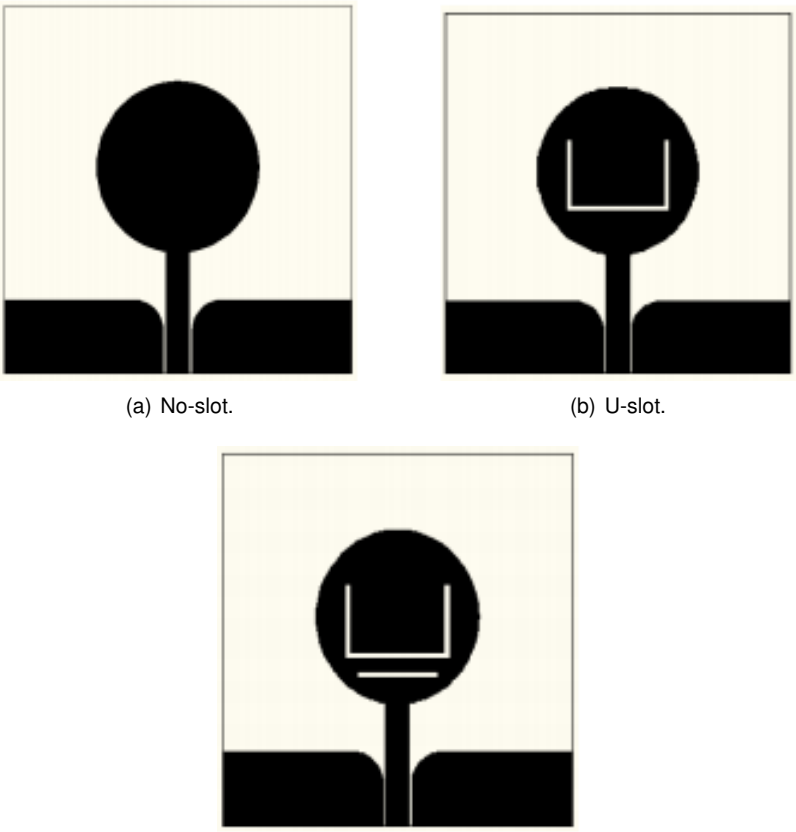

(a) No-slot.

(b) U-slot.

(c) U-slot and line-slot.

Figure 2.9: CPW-fed transparent antenna with multiple slot configuration.

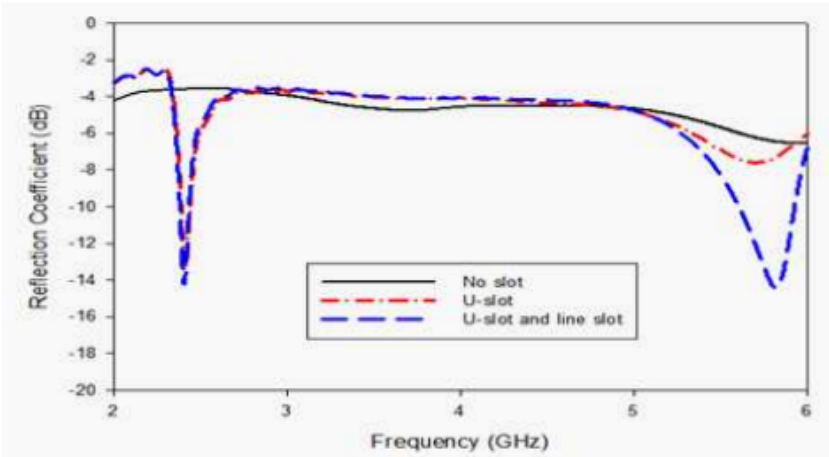

Figure 2.10: Reflection coefficient simulations for the cases in which the proposed antenna has no slots, a U-slot and the combination of an U-slot with a line-slot.

The proposed dual-band requirement was achieved with the combination of the U-slot with the line-slot. Figure 2.11 shows the current distribution along the patch, simulated using the CST^{TM} software. The current concentration observed in Figure 2.11(a) at the top edges of the U-slot indicate that it is responsible for the enhancement observed in the $|S_{11}|$ parameter at 2.45 GHz, comparing to the

Frequency [GHz]	Reflection Coefficient [dB]	Bandwidth ($-10dB$ criteria) [MHz]	Maximum Directivity Gain [dBi]
2.45	-14.2	50	2.2
5.8	-14.4	350	6.38

Table 2.2: Summarized results of the research presented in [55].

situation in which no slots were added. Following the same logic, the current concentration observed in Figure 2.11(b) at the edges of the line-slot explains the improvement detected in the reflection coefficient at 5.8 GHz.

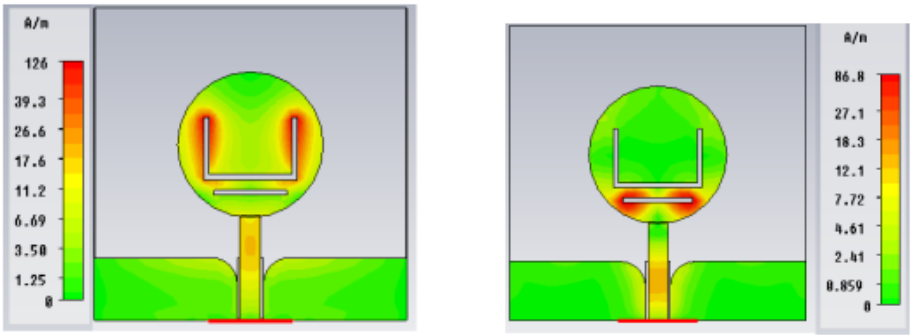

(a) 2.45 GHz, (b) 5.8 GHz.

Figure 2.11: Surface current distribution at:

In this subsection, a compact CPW-fed dual-band transparent antenna, operating at 2.45 GHz and 5.8 GHz was analysed. The introduction of slots has been proved crucial to achieve the aimed resonance frequencies. The proposed antenna managed to be properly designed, in terms of the expected performance in return loss, gain, efficiency and radiation pattern. The reached results are summarized in Table 2.2. The compactness, transparency and ease of fabrication of the proposed antenna makes it a favourable candidate for WLAN applications.

2.3.3 UWB Antennas

Another interesting solution for WBAN applications is the UWB technology. Antennas that operate within this frequency range benefit from an immense amount of bandwidth available, which allows for high data rate radio communications. On top of that, the transmit power is quite low, which is a desired feature in terms of battery consumption, regarding devices that are made with the purpose of being used or carried by an user [29]. However, these types of antennas present a high sensitivity to the influence of the human body, and therefore need to be carefully design in other to improve the quality of WBAN links. On that note, a coplanar-fed planar monopole UWB antenna is presented in [30] for off-body communications and to be used in the vicinity of the human body. The antenna is shown in Figure 2.12. The antenna dimensions are defined in Table 2.3. The substrate employed is $RT/Duroid^{TM}5880$, which is characterized by having 1.57 mm thickness, relative permittivity $\varepsilon_r = 2.2$ and a loss tangent $tan\delta = 0.0009$.

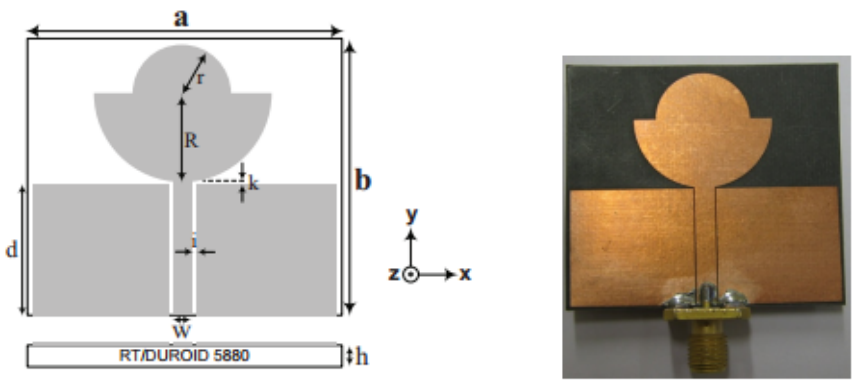

(a) Antenna geometry and parameters. (b) Printed antenna.

Figure 2.12: Example of a CPW UWB monopole antenna.

a	b	R	r	d	w	k	i	h
44	38	11	7.5	18	3.2	0.2	0.15	1.57

Table 2.3: Summarized results of the research presented on [30].

The antenna was simulated with the High Frequency Structure Simulator ($HFSS^{TM}$) software, and is essentially composed of a radiating patch composed on its top by two semicircles, one with a radius bigger than the other. The current distribution was firstly analysed and depicted at strategic frequencies, as can be seen in Figure 2.13. It is clear that the areas where the current is more concentrated (in the top edges of the ground plane and along the sides of the bigger semicircle), are the ones to be more carefully examined, as any deviation from their optimized dimensions is more likely to affect the antenna impedance bandwidth. Therefore, the dimensions of the radiator patch and the radius of the bigger semicircle are the main variables to be taken into consideration. Figure 2.14 illustrates the effect of changing the value of the R parameter (variable used by the author to define the radius of the biggest semicircle). The less that value is, compared to its fixed value (detailed in Table 2.3), the more the magnitude of the reflection coefficient is decreased. This points out the fact that the radii of the semicircles can be used to directly regulate the impedance bandwidth of the antenna.

The next step was to evaluate the behaviour of the antenna when in presence of a human user. The author decided to use the two simplified models represented in Figures 2.1(a) and 2.1(b) instead of whole-body models, so to greatly reduce the computational time taken by the simulations. The $|S_{11}|$ parameter was measured both in free space (Figure 2.15(a)) and on the arm of a human user (Figure 2.15(b)). The measurement setup is portrayed in Figure 2.15. The measures performed next to the arm were carried out acknowledging a space between the arm and the antenna. As a solution, the author used a small strip of polyethylene amidst the arm and the antenna, as well as a latex band wrapped around the arm to fix the position of the antenna, so it would not be another factor that could alter the measuring results.

The obtained results are graphically depicted in Figure 2.16. In Figure 2.16(a), the results shown are the outcome of the simulation using the $HFSS^{TM}$ software, comparing the scenarios in which the antenna is put next to a simplified flat model of a human arm, and next to a simplified elliptical model

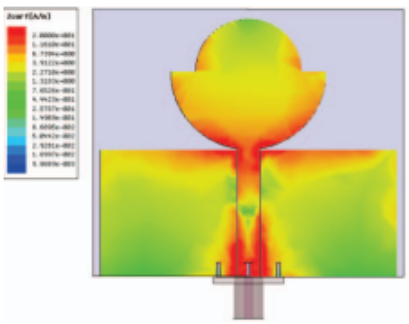

(a) At 3.5 GHz.

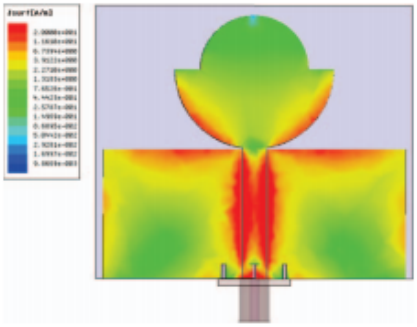

(b) At 7.2 GHz.

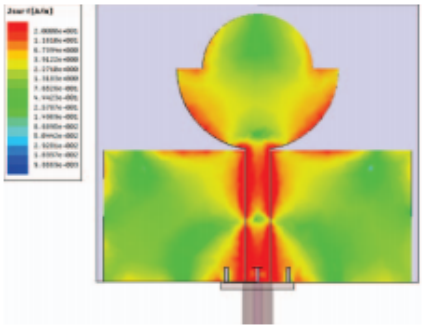

(c) At 11 GHz.

Figure 2.13: Current distribution.

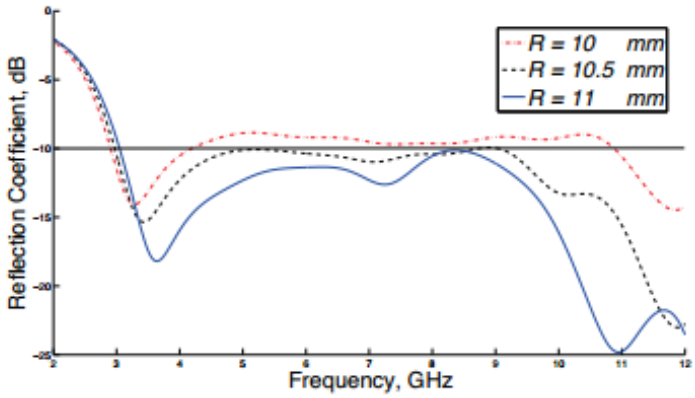

Figure 2.14: Simulated reflection coefficient as a function of the radius of the biggest semicircle, with the parameters from Table 2.3 fixed.

of the human arm, both placed at the same distance from the antenna. It can be seen that the elliptical model has a slighter effect on the impedance bandwidth, comparing to the flat model. Figure 2.16(b) shows the results of simulating the antenna in free-space, reached with the simulator and in laboratory. The frequency range chosen was between 2 and 12 GHz, and the results showed that the antenna has an impedance bandwidth that verifies the $-10dB$ criteria, ranging from 3.05 to beyond 12 GHz. Figure 2.16(c) illustrates the measured and simulated reflection coefficient for two different situations, one with the antenna separated from the human arm by 3 mm, and the other with the antenna distanced by 7 mm. The attained measured and simulated results are congruent. The further the antenna is placed with respect to the human arm, the more the results approach the ones obtained for the free-space case.

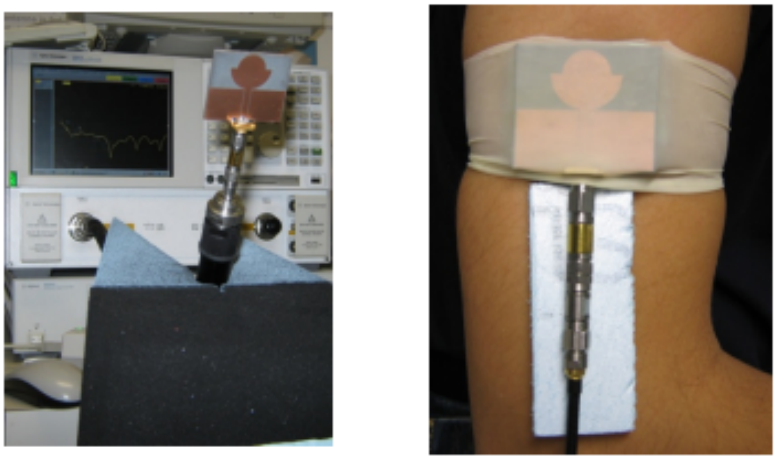

(a) In free-space. (b) On a human arm.

Figure 2.15: Measurement setup of the CPW UWB monopole antenna.

Also, the comparison between the measured and simulated results shows that the simplified elliptical shaped model is more than suitable to study the behaviour of the designed and developed antenna in the vicinity of a human limb.

A CPW-fed antenna was presented in this subsection for UWB off-body applications and to be used next to the human body. An elliptical simplified model of a human arm was seen to be perfectly capable of predicting the performance of the antenna in the proximity of a human user. However, in the whole UWB spectrum there are areas in which the $-10dB$ criteria is not verified, as it can be seen in Figure 2.16 around 5, 7 and 9 GHz (for the situation in which the antenna is separated from the human arm by 3 mm). The author went on and deepened the investigation on the current antenna, as can be read about in [29]. The author of this dissertation proceeded to improve the antenna presented on this subsection, notwithstanding, as it will be demonstrated in the following chapter.

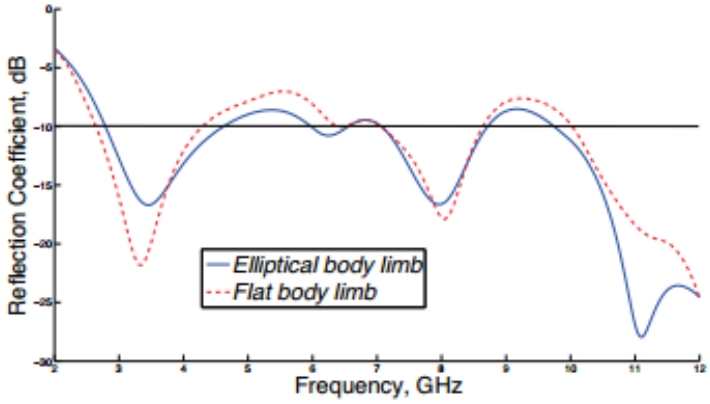

(a) Effect of simplified models on the antenna impedance bandwidth.

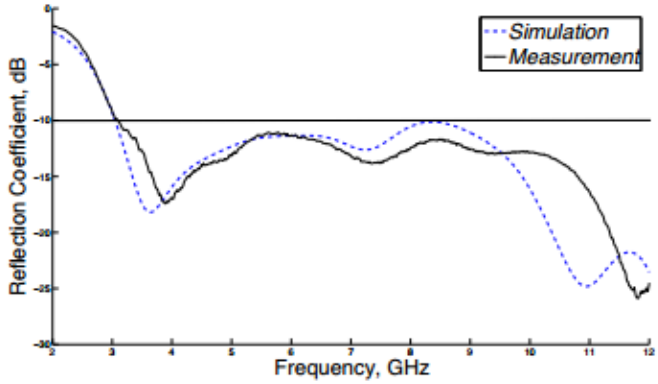

(b) Measured and simulated reflection coefficient in free-space.

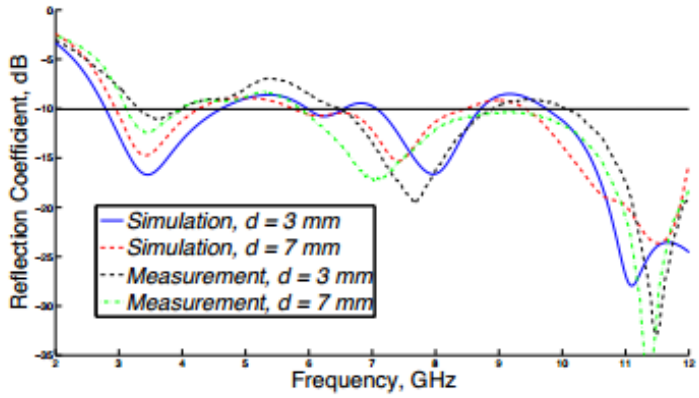

(c) Measured and simulated reflection coefficient in the vicinity of a human arm.

Figure 2.16: Measured and simulated $|S_{11}|$ parameter for different scenarios.

Chapter 3

Design of a dual-band antenna operating at ISM bands (2.45 GHz and 5.8 GHz) and an UWB antenna

The main objective of the dissertation is to design a mechanically robust dual-band antenna, which operates in the ISM bands of 2.45 and 5.8 GHz, and is quasi-immune to frequency detuning when in presence of a human user (because real conditions do not permit the perfecting matching between simulated and measured results). An UWB antenna is also designed and simulated, with the sole purpose of studying a different approach, both in terms of operating frequencies and feeding solutions. Throughout this chapter, the whole process that led to the final formats of the antennas is detailed, from the basic gathering of information to the simulation of the most critical parameters of the antennas, that describe their behaviour. In the end, the simulation results are exhibited, and an analysis on them is carried out.

3.1 Microstrip Patch Antennas

In subsection 2.3.2, the antenna designed in [55] served as an inspiration to the antenna developed in this dissertation, as it proposed a configuration that allows the designer to fix the pretended resonance frequencies. But first, the microstrip solution employed came from several papers that are present in the literature. The increasing usefulness of a microstrip patch antenna due to their low cost, low profile, light weight, flexibility in terms of electromagnetic parameters, ease of fabrication, conformability to planar and non-planar surfaces and possible dual-frequency operation presented itself as a starting point for designing a robust antenna for WBAN applications. So firstly a microstrip antenna was studied and then several configurations were simulated.

Figure 3.1 shows a simple illustration of a microstrip antenna. The latter is fed by a microstrip transmission line and constituted by a patch antenna and a ground plane, all made of a metal of high

conductivity (copper was employed in the fabricated designs). The patch is of length L, width W, and between the patch and the ground plane there is a substrate of thickness h and permittivity ε_r.

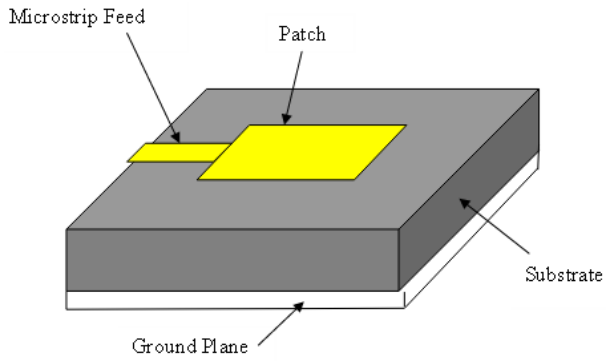

Figure 3.1: Microstrip Antenna.

There are several parameters that are dependent on the measures of the patch antenna. Equation 3.1 helped with the dimensioning of the developed antennas:

$$f_c \approx \frac{c}{2L\sqrt{\varepsilon_r}} \tag{3.1}$$

where f_c is the operating frequency, c the speed of an EM wave in vacuum, L the length of the patch antenna and ε_r the permittivity of the dielectric circuit board (substrate). As one can observe from equation 3.1, the higher the length of the patch, the lower the operating frequency, so the former can be seen as a way of controlling the resonant frequency.

Next, the operational principles of a conventional rectangular microstrip patch antenna are described. Firstly, the length L should be around one half of the wavelength, so the antenna is resonant [68] [49]. This characteristic is fundamental, because it is what makes the antenna radiate, and achieve a maximum in the z direction (one wants the antenna to radiate perpendicularly to the body, which is crucial for off-body communications). Therefore, the antenna can be seen as a $\lambda/2$ transmission line resonant cavity with two open ends. With an open circuit end, the current at the end of the patch will be zero and maximum at the center of the patch (at $\lambda/2$), making it theoretically zero at the beginning of the patch (see Figure 3 of [49]).

Another important aspect is the behaviour of the electric field inside the dielectric. Being a half wave long patch, the electric field goes from a maximum (and positive) value at the beginning of the patch, to zero, at the middle, to a minimum (negative value) at the end. Of course, these values are constantly varying in amplitude and sign, but they do not end exactly at the edges of the patch; the electric field is 'spilled' out of those frontiers (see Figure 3.2). This is called the fringing effect. The fringing fields between the periphery of the patch and the ground plane are responsible for making the antenna radiate.

Bearing in mind that the fringing effect makes the microstrip patch antenna seem electrically wider compared to its physical dimensions (see Figure 3.2(c)), the rectangular patch antenna can now be fully characterized.

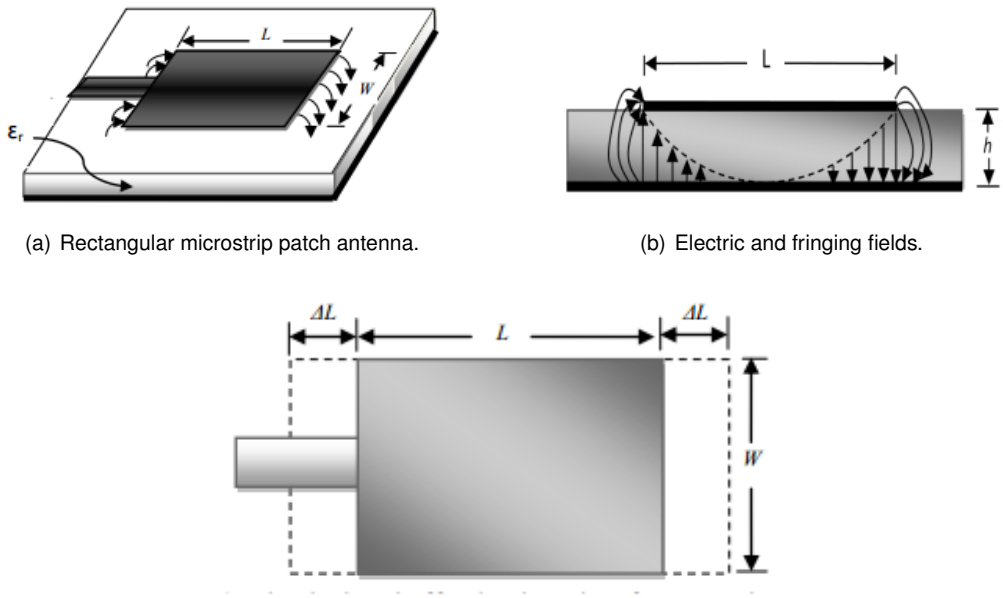

(a) Rectangular microstrip patch antenna.

(b) Electric and fringing fields.

(c) Physical and effective lengths of the rectangular microstrip patch.

Figure 3.2: Fringing effect, retrieved from [13].

$$\varepsilon_{eff} = \frac{\varepsilon_r + 1}{2} + \frac{\varepsilon - 1}{2}\left(1 + \frac{12h}{W}\right)^{-\frac{1}{2}} \tag{3.2}$$

Equation 3.2 translates the concept of effective dielectric constant. The latter was introduced due to the fact that the spilled electric field waves travel in both dielectric and air, as can be seen in Figure 3.2(b). Having that defined, one can address Equation 3.3 to calculate the electrical length that extends the physical length L of the patch:

$$\Delta l = 0.412h\left(\frac{\varepsilon_{eff} + 0.3}{\varepsilon_{eff} - 0.258}\right)\left(\frac{\frac{W}{h} + 0.264}{\frac{W}{h} + 0.8}\right) \tag{3.3}$$

where $\frac{W}{h}$ is the patch width to substrate height ratio. The effective length can also be determined by Equation 3.4, as it is a length seen from an electric perspective:

$$L_{eff} = L + 2\Delta l \tag{3.4}$$

where L is the physical length of the patch. Finally, the width W of the patch antenna is also of great importance, as it can directly affect the input impedance, the radiation pattern and even the bandwidth [68] [49]. An optimized width for an efficient radiator can be given by Equation 3.5:

$$W = \frac{c}{2f_c}\left(\frac{\varepsilon_r + 1}{2}\right)^{-\frac{1}{2}} \tag{3.5}$$

with f_c corresponding to the pretended resonant frequency.

When the substrate is chosen, and so one has already the dielectric permittivity and the height selected (according to the available material), as well as the desired working frequency, the above

formulas can be used to design the antenna. Once that is achieved, the critical parameters of the antenna, such as return loss, radiation pattern and efficiency can be investigated.

3.1.1 Return Loss

The return loss is quite an important parameter of an antenna, and therefore must be carefully investigated, as it can define if an antenna is functioning or not. The magnitude of the reflection coefficient, $|S_{11}|$, serves as a measure of the effectiveness of an antenna, regarding the amount of transmitted power that is reflected and thus not availed. Equation 3.6 translates the ratio between the reflected power and the incident power [7]:

$$|S_{11}|_{dB} = 10log_{10}\frac{P_r}{P_i} \tag{3.6}$$

in which P_i and P_r refer to the incident power of an antenna and to the power that is reflected by the source antenna, respectively.

As mentioned above, the return loss defines if an antenna is working or not. This means that according to a certain criteria the operation band of an antenna is defined as the range of frequencies where the antenna is tuned [7]. One way to do that is to adopt the conventions referred to in subsection 2.3.1, and see which one is suitable for the antennas in study.

3.1.2 Radiation Pattern

The radiation pattern of an antenna is a graphical representation of how the antenna is radiating in certain directions [7] [40]. It is usually observed in the far-field region, and measures the radiated power by an antenna as a function of the arrival angle. Figure 3.3 represents the set of coordinates that is generally used to represent the radiation pattern of an antenna. In the latter the standard spherical coordinates can be distinguished: the angles θ (theta) and ϕ (phi). The former is measured off the z axis, while the latter is measured off the x axis.

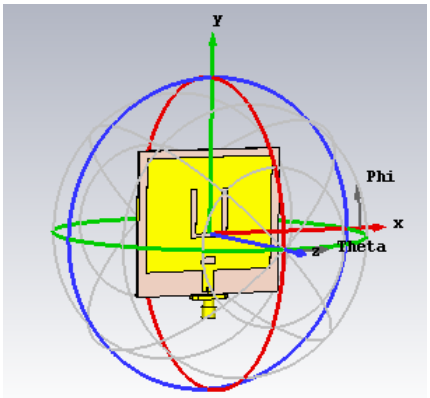

Figure 3.3: Set of coordinates necessary to determine the radiation pattern.

An example of two and three-dimensional radiation patterns is portrayed in Figures 3.4(a) and 3.4(b), respectively. It is from the radiation pattern that one can extract information regarding how an antenna

directs the power that is radiating. If the radiation pattern is the same in all directions, the pattern is called isotropic. This pattern does not actually exist (it is ideal), but usually the directivity of real antennas is compared to the one with an isotropic radiation pattern, and therefore their directivity is expressed in dBi, with the i standing for the relation to the isotropic antennas. A second pattern can also be mentioned, the omnidirectional one. This means that an antenna has an isotropic pattern in a single plane. It can be seen in antennas that have a doughnut-shape or toroidal radiation pattern, such as dipoles or slot antennas.

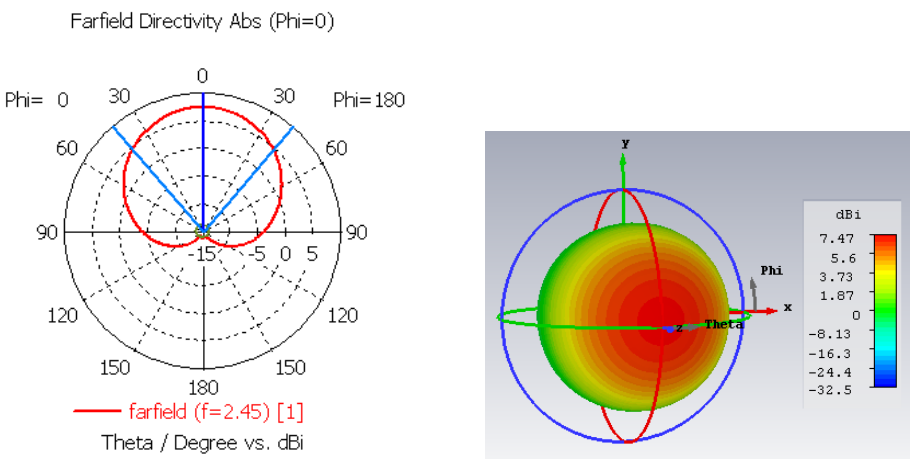

(a) Two-dimensional radiation pattern.

(b) Three-dimensional radiation pattern.

Figure 3.4: Radiation pattern of an antenna, in 2D and 3D.

The most common types of antennas are the ones that do not have a symmetrical pattern. These antennas are called directional, and have an evident peak of radiation towards certain directions. The patch antenna is one case, and its directivity can be easily estimated through Equations 3.7 and 3.8 [68] [44]:

$$D \approx 6.6(8.2dBi), \quad for \quad W \ll \lambda_0; \tag{3.7}$$

$$D \approx 8W/\lambda_0, \quad for \quad W \gg \lambda_0. \tag{3.8}$$

Of course, there are ways to improve the directivity of a patch antenna. Assuming one separated from a ground plane by a substrate, and that the ground plane is 'infinite', all radiation would occur in just one half (in the case of Figure 3.4 the antenna would only radiate for $z > 0$). This would be translated in a perfect front-to-back ratio (with no radiation towards the back). But then again, there is no such thing as an infinite ground plane (another ideal situation), although the previous illustration serves to highlight the importance of the size of the ground plane if one wants a highly directive antenna. Also, since this dissertation evaluates the behaviour of the antennas when exposed to the human body, to have a great front-to-back ratio is quite important, as no radiation should be emanated to the user, preferably. This will be further discussed, taking into account the SAR parameter.

3.1.3 Efficiency of an Antenna

The efficiency of an antenna can be simply stated as the ratio of the power that is delivered to it and the power that the antenna radiates [10]. To have a highly efficient antenna is to have its input power mostly radiated away, whereas a low efficiency antenna 'sees' its input power absorbed or reflected away. Also, the antennas are reciprocal; this property states that the antenna in its transmitting mode behaves exactly as it were in its receiving mode, meaning that antennas do not have distinct transmit and receive radiation patterns. Therefore, the efficiency of an antenna (also designated for radiation efficiency) can be mathematically described as:

$$\varepsilon_{rad} = \frac{P_{rad}}{P_{in}} \tag{3.9}$$

where P_{rad} is the power radiated by the antenna, and P_{in} the power delivered to it. Equation 3.9 denotes ε_{rad} as the radiation efficiency; it is called that way to differentiate from another type of efficiency of antenna (the one that usually people refer to when they just say 'efficiency'), which is total efficiency. The latter takes into account the losses due to impedance mismatch, when connected to transmitting or receiving equipment. Equation 3.10 expresses the relation between total efficiency and radiation efficiency:

$$\varepsilon_{total} = M \times \varepsilon_{rad} \tag{3.10}$$

with M representing the losses of an antenna due to impedance mismatch, and comprises a number from 0 to 1.

There are several factors that can also contribute to the reduction of the (total) efficiency of an antenna. For example, the finite conductivity of the metal employed to build the antenna leads to conduction losses; the non-zero electrical conductivity of the dielectric used for the substrate generates heat that weakens the energy of the electric fields that surround the antenna [10]. These are all factors which the antenna designer can not do anything about (but to choose materials that possess parameters that do not decrease the efficiency of an antenna significantly), so in order to obtain a highly efficient antenna one should look for ways to improve the impedance mismatch losses.

3.2 Design of a Dual-Band Antenna

Taking into account the antenna detailed in subsection 2.3.2 and all the considerations approached in section 3.1, the design and development of a dual-band antenna that operates in the ISM band is presented in this section. The designed antenna is printed photolithographically on $RogersRT/Duroid^{TM}5880$, with thickness h of 1.57 mm, relative permittivity ε_r of 2.2 and loss tangent $tan\delta$ of 0.0009 (more detailed information on this material can be found in [59]).

The Rogers material was chosen so to overcome certain limitations of a microstrip antenna [31] and to make it cost-effective. The selection of an adequate substrate is crucial, as its parameters influence

the bandwidth, efficiency and radiation pattern of a patch antenna. The $RogersRT/Duroid^{TM}5880$, besides being designed for microstrip circuit applications [59], offers a suitable trade-off between bandwidth and gain [31] [54]. The thickness of 1.57 mm is big enough to provide mechanical robustness to the antenna and at the same time small enough to let the antenna be easily integrated with other microwave circuits and minimize surface wave propagation. The latter comes from electromagnetic propagation modes that are trapped in-between the dielectric [56]. These so called surface waves travel along the dielectric through successive reflections, and at the edges of the patch they may interfere with the primary waves that are radiated by the patch, degrading the performance of the antenna.

The low dielectric constant and dielectric loss are also appropriate for the following development of the antenna. The lesser the losses in the dielectric (here parametrized in terms of the tangent of the loss angle, $tan\delta$) the lesser the input power will be dissipated. Since the designed antenna is to be used in the vicinity of the human body, and for off-body communications, one must make sure the radiation is maximum in the direction off the body (later on assumed as the z direction), which can be achieved by having a substrate with a low permittivity [39].

With the substrate chosen, one moves to the next step: the dimensioning of the patch. The envisioned antenna would be a dual-band one, so the author of this dissertation decided to scale out a rectangular microstrip patch antenna, as it has been described until here, to operate at the ISM band of 2.45 GHz. After, a slot would be introduced so to provide the second working band, of 5.8 GHz [32] [41] [53] [19] [43] [34] [35] [36] [55] [40].

In Figure 3.5, the format that served as a 'canvas' to attain the final design is portrayed. A rectangular microstrip patch antenna, dimensioned to operate at 2.45 GHz. To note that all the antennas presented throughout this section have an architecture that is the result of several sweeps performed to each measure parameter with $ParameterSweep$ of $CST^{TM}MicrowaveStudio$, and of various optimizations using the $Optimizer$ tool of the same software. The optimized measures are obtained according to the established primary goals, which are to achieve return loss values below -10 dB for the working frequencies. The simulation are also carried out including a connector, which has its construction detailed in Appendix A.

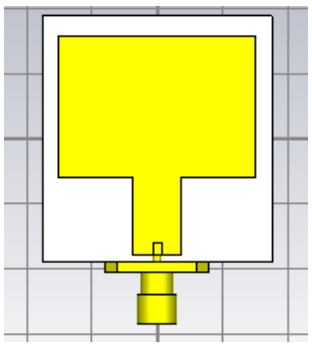

Figure 3.5: Microstrip patch antenna.

From that, several ideas were modelled, and different solutions were explored. From various articles displayed in the literature, the author chose to focus on line and U-slots. These are well studied and common solutions employed to overcome some limitations of the microstrip solution (such as narrow-

bandwidth [41]) and to facilitate the introduction of more resonance frequencies [32] [53] [55]. Assorted models were conceived in other to evaluate the performance of the antennas according to changes in their dimensioning. Figure 3.6 shows two different antennas design with the $CST^{TM} MicrowaveStudio$ software.

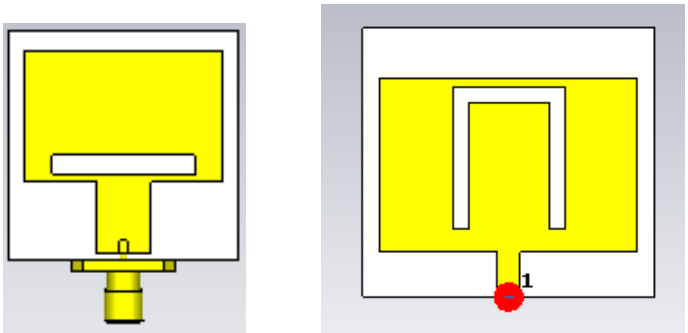

(a) Rectangular microstrip patch antenna with line-slot.

(b) Rectangular microstrip patch antenna with U-slot.

Figure 3.6: Different slots in patch antennas.

Both antennas operate in the ISM bands of 2.45 and 5.8 GHz. The obtained results for each one are discriminated in Figures 3.7, 3.8 and 3.9. Here, attention was paid to certain features: the effect of having a ground plane smaller than the substrate (just like in [67]), the effect of the introduction of a line-slot or of an U-slot, and the radiation pattern. The latter is due to the fact that, as previously mentioned, one requires the antenna to radiate away from the user (in the z direction).

Firstly, and in order to introduce a topic that is going to be further explained, Figures 3.7(a) and 3.7(b) exhibit the choice of a ground plane that does not fully cover the substrate (with more precisely one fifth of the length of the substrate), and the $|S_{11}|$ parameter of the antenna, respectively. Here, the length of the ground plane was varied for different simulations, and the return loss shown is the one that translates the best results, showing two perfectly functional operating bands at 2.45 and 5.8 GHz, as according to the goals envisioned for the antenna.

The dual-band fashion is achieved with the insertion of a line-slot on the patch. The rectangular patch was firstly parametrized to operate at 2.45 GHz, and the introduction of a well-dimensioned line-slot allowed the appearance of another resonance frequency, at 5.8 GHz, as it can be seen by the current distribution in Figure 3.8(a), with the current being mostly concentrated at the edges of the slot. Figure3.8(b) confirms that observation, by comparing the $|S_{11}|$ parameter for the case with no-slot (in green), in which the microstrip patch antenna was designed to solely operate at 2.45 GHz, and the case with a line-slot (in red), evidencing the introduction of a new resonance frequency at 5.8 GHz.

Figure 3.9(a) perceives as well the goals established, that predicted a radiation pattern with preferably a maximum in the z direction (meaning that one wants the radiation direction to be normal to the front-side of the patch). However, one small observation invalids the whole process; although the simulated results seem to fulfil the settled requirements for the dual-band antenna, Figure 3.9(a) also shows it radiates with the same intensity to the opposite side, resulting in an unsatisfactory front-to-back ratio. This is an undesirable behaviour when one wants to further put the antenna on a human user because

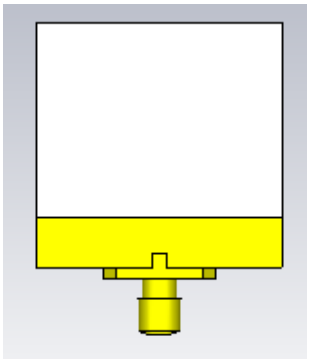

(a) Rear-view, showing a rectangular ground plane with a length that is one fifth of the one of the patch.

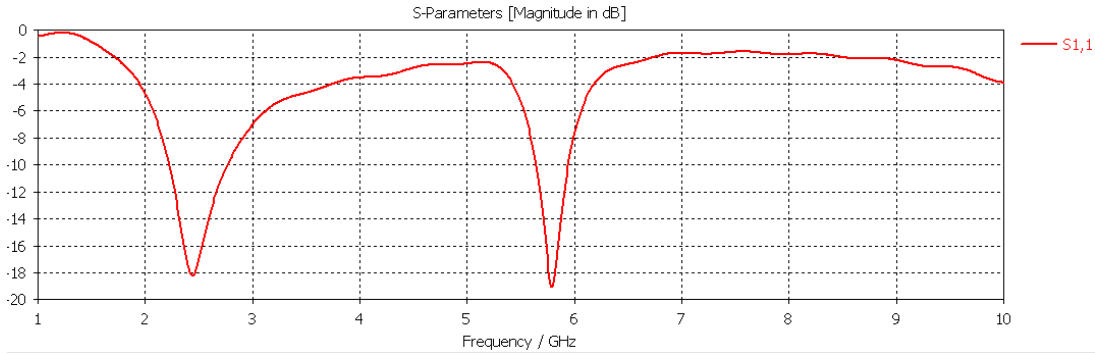

(b) $|S_{11}|$.

Figure 3.7: Simulated results for a patch with a small ground plane and a line-slot.

it results in radiating in the direction of the human tissues, which can lead to possible dangerous SAR values (above the established limits [20]). The same applies to Figure 3.9(b), which to makes things worse radiates in parallel with the human body.

The author pursued the approach of the previous example, by using a ground plane with the same measures of the substrate, but after several attempts, with the help of the $Optimizer$ and $ParameterSweep$ tools from $CST^{TM}MicrowaveStudio$, it was not possible to fix the operating bands at 2.45 and 5.8 GHz (the best results managed working frequencies at 2.45 and 5.2 GHz, but since the second band was not of interest to this work, that solution was discarded). The author moved on to the next configuration: insertion of an U-slot. Figure 3.10(a) shows the effect of the inverted U-slot through its current distribution, and Figure 3.10(b) shows the $|S_{11}|$ parameter of the antenna from Figure 3.6(b).

Figure 3.11 compares the $|S_{11}|$ parameter for the case with no-slot (in red) and for the case with an inverted U-slot (in green). Although the bandwidth at 2.45 GHz decreases significantly, the inverted U-slot is in fact responsible for the appearance of a resonance frequency at 5.8 GHz.

In terms of radiation pattern, the inverted U-slot does not interfere with the lower resonance frequency of 2.45 GHz, as it can be seen in Figure 3.12(a). At 5.8 GHz, the current is concentrated within the area delimited by the slot, creating a smaller rectangular patch (see Figure 3.10(a)). This can be seen as a patch within a patch (in terms of current distribution), with dimensions similar to the ones that would be attained (with the help of the equations described in section 3.1) if one were to design a rectangular

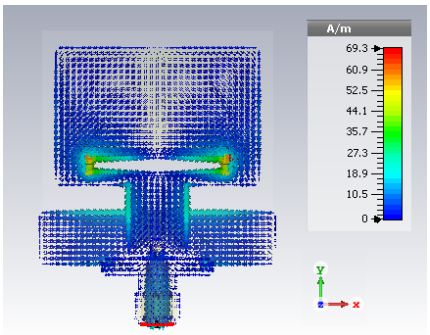

(a) Current distribution at 5.8 GHz.

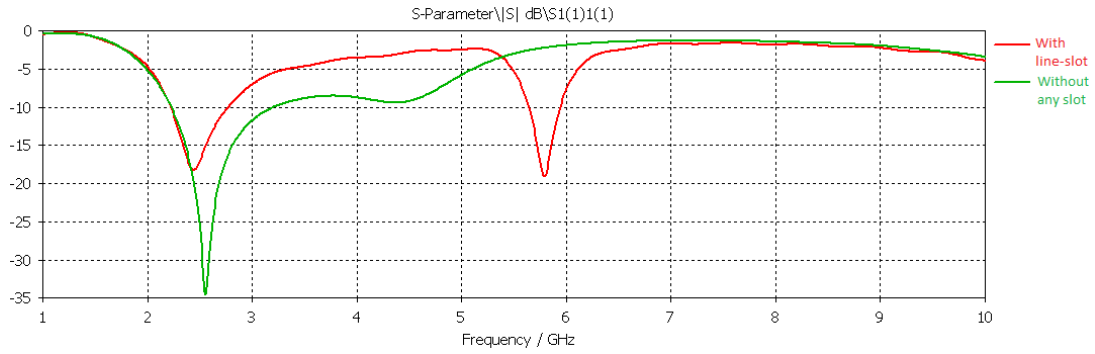

(b) Comparison of the $|S_{11}|$ parameter for the case with no-slot and with line-slot.

Figure 3.8: Appearance of a new frequency band by introducing a line-slot on the patch antenna.

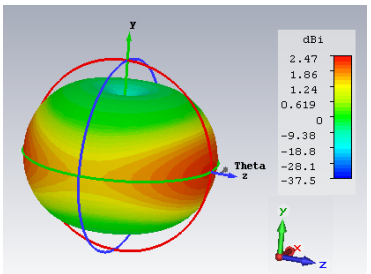

(a) Radiation pattern at 2.45 GHz.

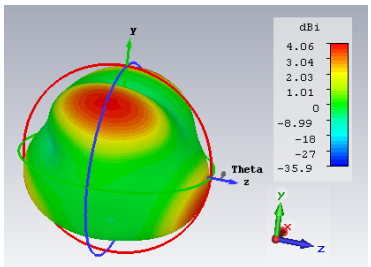

(b) Radiation pattern at 5.8 GHz.

Figure 3.9: Radiation pattern of a dual-band antenna with a line-slot, illustrated by Figure 3.6(a)

microstrip patch antenna to operate at 5.8 GHz.

However, once again the radiation pattern does not correspond to the pretended behaviour of the antenna. Although the radiation pattern at 2.45 GHz (see Figure 3.12(a)) is suitable according to the set objectives, the radiation pattern observed in Figure 3.12(b) at 5.8 GHz indicates that the antenna does not radiate in the z direction, making it a 'deal-breaker'. The current distribution seen in Figure 3.10(a) shows the destruction interaction of currents that come from opposite sides, which causes the patch to not radiate in that part (which is where a maximum of current concentration would be coveted), and thus radiate away from it in other directions.

Just as a note, an attempt for the more common solution of an U-slot, instead of an inverted one, was studied, but the author had no success in fixing the desired frequency bands. Therefore, the following idea was to combine the two slots mentioned throughout this section. From [43], [34] and [36] emerged

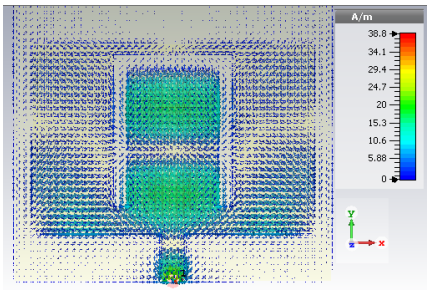

(a) Current distribution at 5.8 GHz.

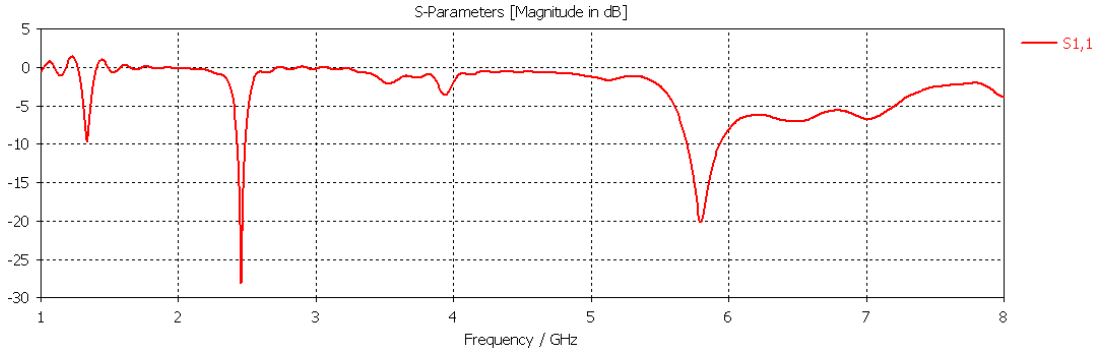

(b) $|S_{11}|$.

Figure 3.10: Appearance of a new frequency band by introducing an U-slot on the patch antenna.

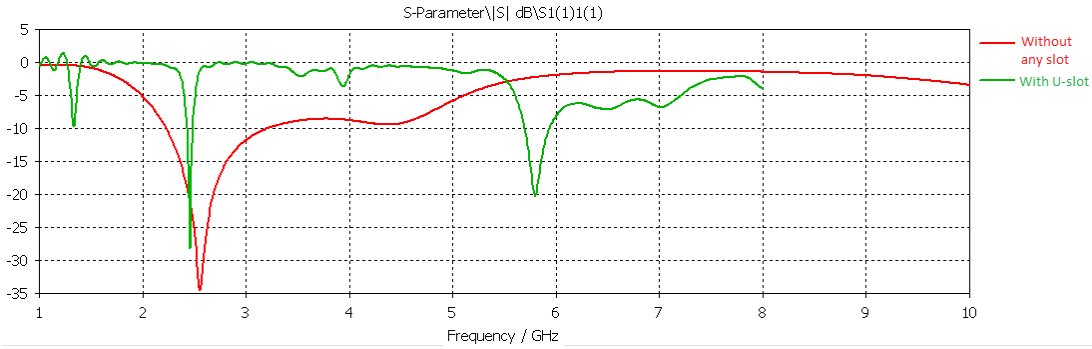

Figure 3.11: Comparison of the $|S_{11}|$ parameter for the case with no-slot and with an inverted U-slot.

the idea of combining more than one slot, keeping the feed simple and remaining in a single-layer and single-patch structure. The antenna from [55], detailed in subsection 2.3.2, demonstrated the possibility of combining both line- and U-slot in the same patch, in order to achieve the working frequencies of the ISM bands. The final design is illustrated in Figure 3.13(a).

The antenna is constituted by a feed line, of $bw \times bl\ mm^2$; a patch of $pw \times pl\ mm^2$; a substrate with $w \times l\ mm^2$ and a layer of copper with the same length and width as the substrate, but with a thickness $th_{copper} = 0.035\ mm$ (see Figure 3.13(b)). The ground plane (and substrate) extend beyond the edges of the patch, both in width and length, so the antenna can operate properly [49] [40]. That extension prevents possible fringing effects and increases the mechanical stability of the antenna. On the feeding side, a gap of $1mm$ was left so to fit the connector and avoid short-circuits. On the patch two cuts are visible: the bigger one, that corresponds to the U-slot, and the smaller one, matching the line slot. The optimized measures are specified in Table 3.1.

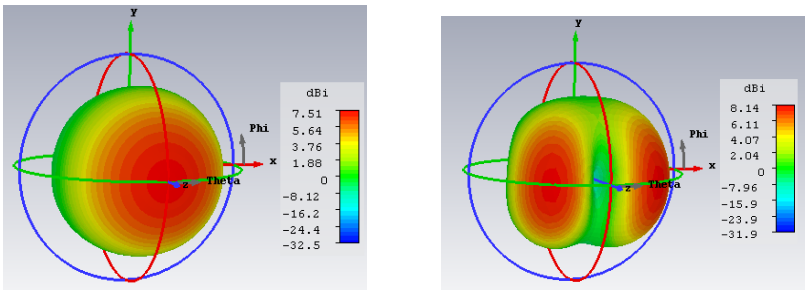

(a) Radiation pattern at 2.45 GHz. (b) Radiation pattern at 5.8 GHz.

Figure 3.12: Radiation pattern of a dual-band antenna with an inverted U-slot, illustrated by Figure 3.6(b).

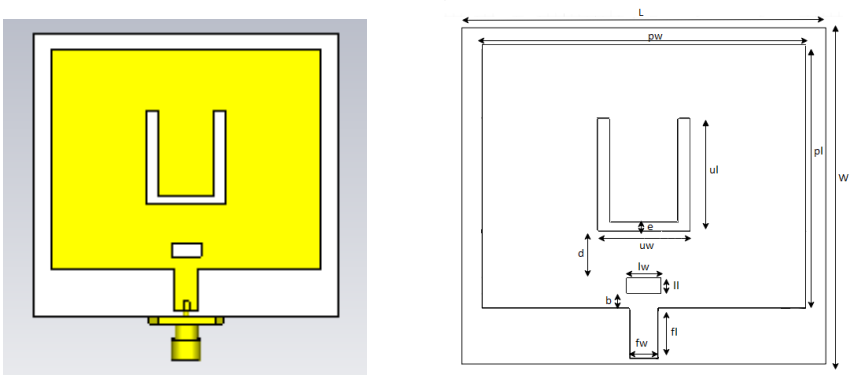

(a) Dual-band antenna. (b) Geometry and design parameters.

Figure 3.13: Dual-band microstrip patch antenna

Next, the main parameters of the dual-band antenna simulated in $CST^{TM} MicrowaveStudio$ are discriminated. Figure 3.14 illustrates the $|S_{11}|$ parameter, with Figures 3.15(a) and 3.15(b) zooming in on the pretended working frequencies. The craved frequency bands are once again attained, with a great margin for work, in terms of magnitude of the return loss.

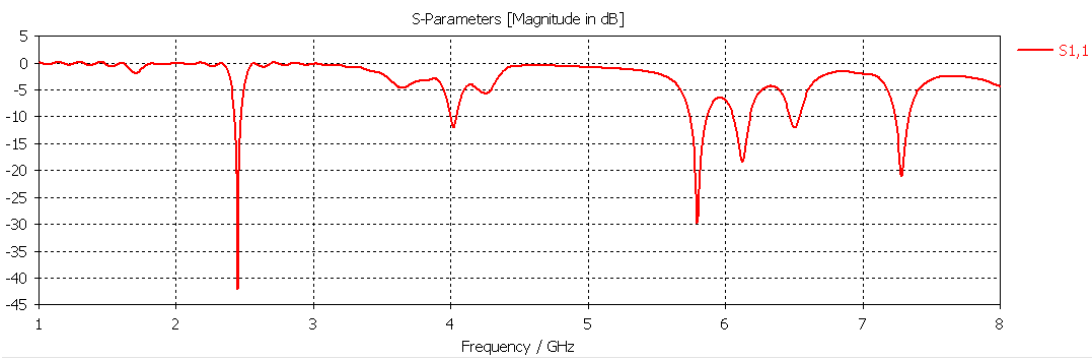

Figure 3.14: $|S_{11}|$ parameter simulated for the dual-band microstrip patch antenna.

Table 3.1: Parameter values, in mm, of the antenna presented in Figure 3.13.

L	W	pl	pw	fl	fw	ll	lw	ul	uw	e	d	b
60	64.95	46.94	57.72	10	5	2.88	6.36	20.16	16.6	1.64	13.71	2.54

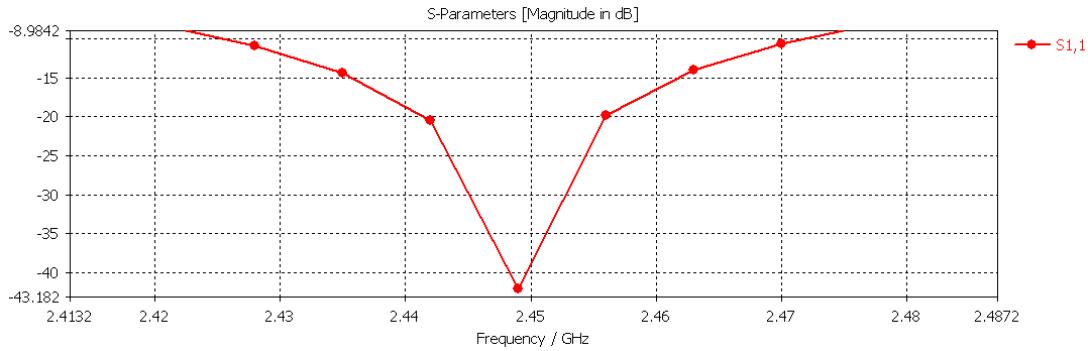

(a) Zoom in on the lower resonance frequency, at 2.45 GHz.

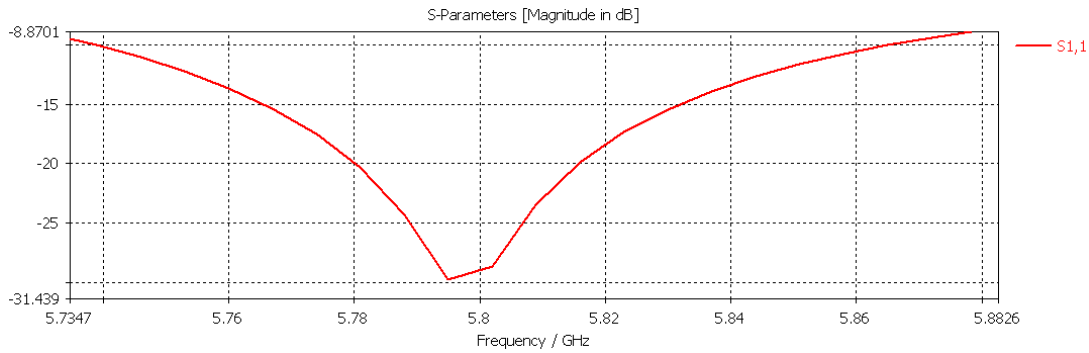

(b) Zoom in on the higher resonance frequency, at 5.8 GHz.

Figure 3.15: Zoom in on the resonance frequencies of the dual-band microstrip patch antenna.

Figure 3.16 depicts the current distribution. Now one can see the difference to the previous design configurations. It is clear now that the U-slot is responsible for the lowest frequency, due to the concentration of current on its edges at that frequency. Any changes on the dimensions of the slot may detune that band. The same applies for the highest frequency: the current is concentrated at the edges of the line-slot, being the latter the accountable for the appearance of that frequency.

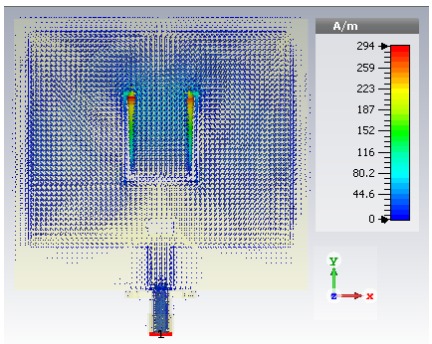

(a) Current distribution at 2.45 GHz.

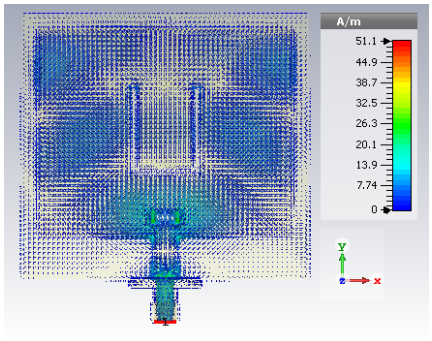

(b) Current distribution at 5.8 GHz.

Figure 3.16: Simulated current distribution of the dual-band microstrip patch antenna.

Finally, all of the requirements are fulfilled. Figure 3.17 depicts the radiation pattern (in 3D) in the desired operating bands. The current distribution of Figure 3.16(a) shows a dispersion of current only around the U-slot, thus making the antenna radiate in the z direction with high directivity (see Figure 3.17(a)). In Figure 3.16(b) the current is dispersed all over the patch, with some destructive interferences

along the way. However, they do not occur in the middle, and the antenna radiates between the line-slot and the U-slot at 5.8 GHz. Although the radiation pattern seems similar to the one achieved in Figure 3.12(b), the antenna does radiate away from the front-side (check directivity in the z direction).

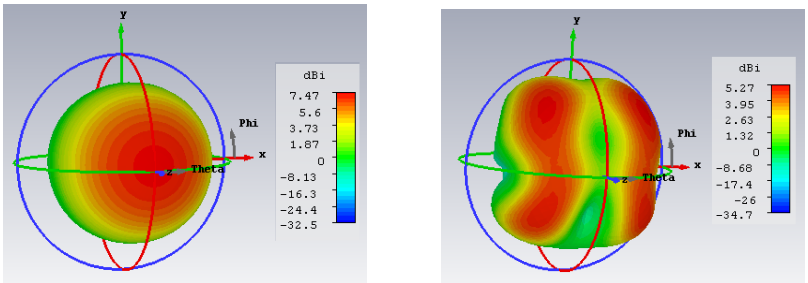

(a) Three-dimensional radiation pattern, at 2.45 GHz.

(b) Three-dimensional radiation pattern, at 5.8 GHz.

Figure 3.17: Simulated radiation pattern of the dual-band microstrip patch antenna.

With this results, the objectives are achieved (in terms of simulation, so far), with the construction of a microstrip dual-band antenna that works at the ISM bands of 2.45 and 5.8 GHz, and radiates away from the body.

3.2.1 Simulation results

The following subsections present a numerical evaluation of the main parameters of the antenna, in terms of simulation purposes, so to describe its performance, which is achieved in a free-space scenario. In Chapter 4 that analysis is accomplished in the vicinity of the human body.

Reflection Coefficient

As explicited in subsection 3.1.1, the return loss is the parameter that quantifies the losses of the power fed to an antenna due to reflection. In this dissertation the author has considered that the antenna is tuned to a certain frequency band when the losses are equal or less than 10% of the input power, which translates into having $|S_{11}|_{dB} \leq 10dB$. Observing Figure 3.15 one can see this criteria is obeyed for the desired resonance frequencies.

Bandwidth

The bandwidth is another fundamental parameter of antenna systems, as it describes the frequency range over which the antennas can radiate or receive power [10]. In [49] several definitions of bandwidth concerning antennas are delineated, but only the so called $impedance/returnlossbandwidth$ is covered, as it is the only one than applies to this work. It stems from an appropriate impedance matching with respect to a particular reference impedance, that permits the appearance of a desired frequency range. Figure 3.18 depicts this concept.

Another way of analysing the bandwidth of an antenna is through a method designated by percent

bandwidth [7] [40]. The latter expresses a normalized measure of the frequency variation that the antenna can handle, and is given by Equation 3.11:

$$BW_{\%} = 200 \times \frac{f_2 - f_1}{f_2 + f_1} \tag{3.11}$$

in which f_2 and f_1 designate the higher and lower frequency limits of the operating bands, respectively (see Figure 3.18(a)). The expression is commonly employed to narrow-band antennas. With all this in mind, the simulated results of the antenna from Figure 3.13(a) are displayed in Table 3.2.

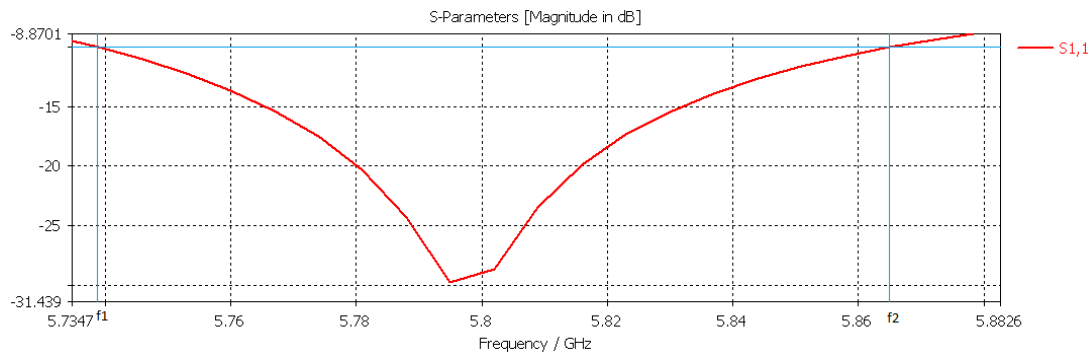

(a) Illustration of the frequency limits of the operating bands.

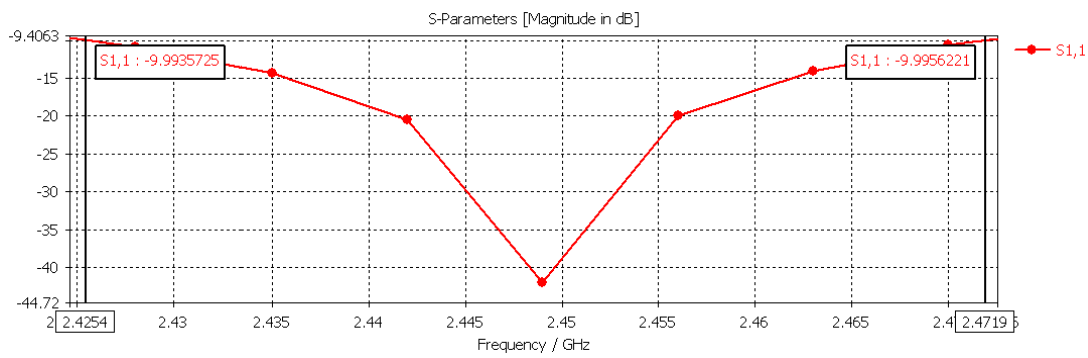

(b) Impedance bandwidth of the operating band with center frequency at 2.45 GHz.

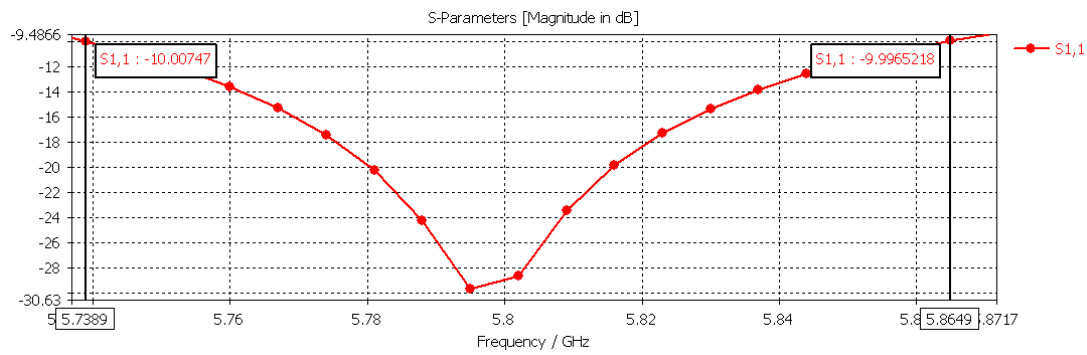

(c) Impedance bandwidth of the operating band with center frequency at 5.8 GHz.

Figure 3.18: Impedance bandwidth.

Frequency [GHz]	Impedance Bandwidth [MHz]	Percent Bandwidth [%]	f_1 [GHz]	f_2 [GHz]
2.45	46.5	1.9	2.4254	2.4719
5.8	126	2.17	5.7389	5.8649

Table 3.2: Simulated results for the impedance and percent bandwidth of the dual-band antenna designed.

Radiation patterns and efficiency

In subsections 3.4 and 3.9 the concepts of radiation pattern and radiation and total efficiency were highlighted. In Figures 3.19 and 3.20, the two-dimensional radiation patterns obtained from CST^{TM} $Microwave\ Studio$ are depicted for the 2.45 GHz and 5.8 GHz bands, respectively, in the xz plane (Figures 3.19(a) and 3.20(a)), in which the ϕ angle is fixed at zero degrees, with θ varying, and in the yz plane (Figures 3.19(b) and 3.20(b)), in which the ϕ angle is fixed at ninety degrees, with θ varying.

From Figure 3.19 one can observe that at 2.45 GHz the antenna is highly directive (7.46 dBi maximum), with a maximum over the z direction, and a very low front-to-back ratio, which is fundamental for this work. The angular width (area in which the antenna radiates with a directivity that varies between its maximum value and half of it) is around eighty degrees, which translates into a wide radiation angle, making it adequate to be used in an area of the body which is not obstructed on the sides (for example, the outer area of an arm).

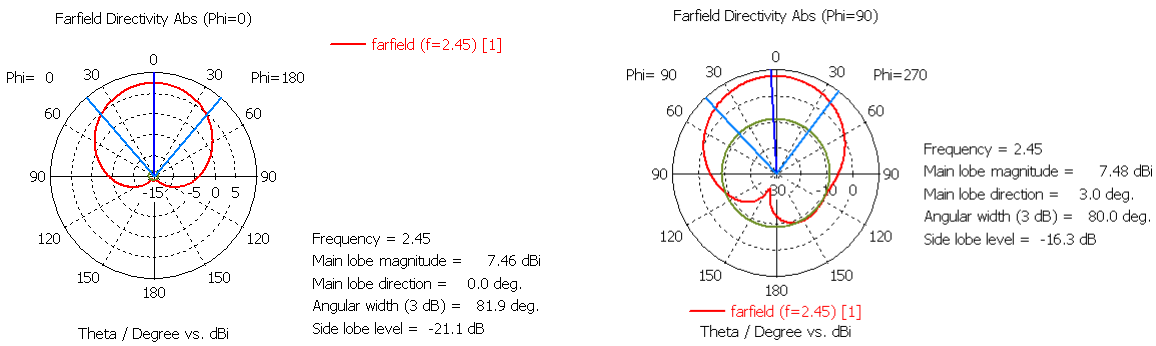

(a) xz-plane radiation pattern, at 2.45 GHz.

(b) yz-plane radiation pattern, at 2.45 GHz.

Figure 3.19: Two-dimensional radiation pattern of the dual-band antenna at 2.45 GHz.

At 5.8 GHz the directivity is much smaller than at 2.45 GHz (see Figure 3.20), however it consists in two main lobes, each at 27 and -27 degrees from the z direction, with a maximum directivity of 4.58 dBi in the xz plane, and a maximum of 2.41 dBi over the yz plane. In the z direction the directivity is around 1 dBi. Nevertheless, the antennas also radiates away from the human body, and still has a low front-to-back ratio.

Regarding efficiencies, the simulated results are depicted in Figure 3.21. Although the figure shows linear graphics, it does not reveal the efficiency increases linearly with higher frequencies; they were only measured for two points (at 2.45 GHz and 5.8 GHz), and by default the $CST^{TM} MicrowaveStudio$ software connects the two dots. As mentioned in subsection 3.1.3, the radiation efficiency measures the

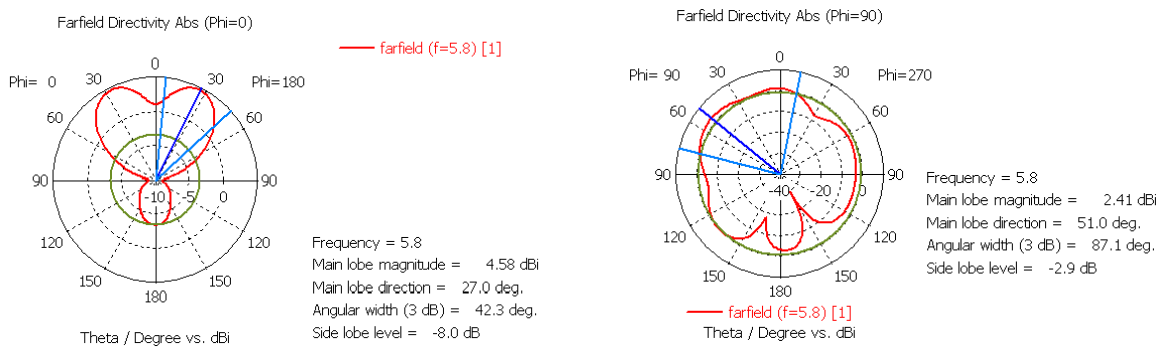

(a) xz-plane radiation pattern, at 5.8 GHz.

(b) yz-plane radiation pattern,at 5.8 GHz.

Figure 3.20: Two-dimensional radiation pattern of the dual-band antenna at 5.8 GHz.

ratio of the radiated power over the one it was provided to it. The total efficiency measures the same, but takes into account the dissipation and the mismatch losses [7].

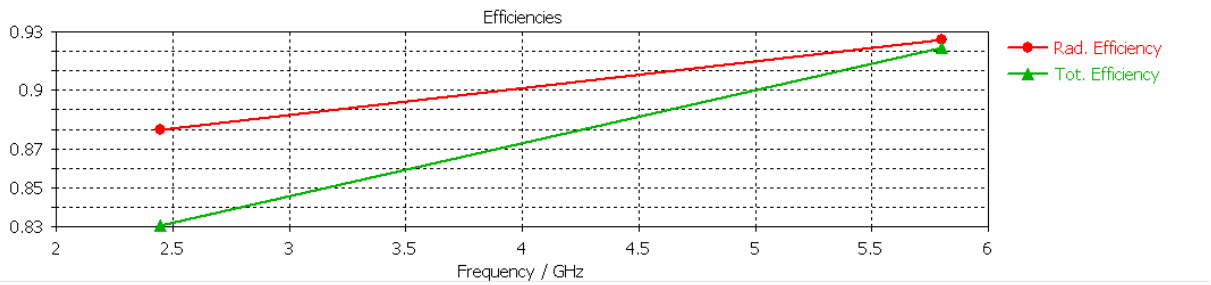

Figure 3.21: Total and Radiation efficiencies simulated for the dual-band antenna.

It can be clearly seen that the antenna shows a high-efficiency conduct, which one can conclude from the 88% and the 92.5% of radiation efficiency at the 2.45 and 5.8 GHz working bands, respectively. The antenna also demonstrates a good impedance matching, with only having 5% of general losses at the lower frequency band, and 0.5% at the higher resonance frequency.

3.3 Design of an UWB Antenna

In subsection 2.3.3 of chapter 2 an UWB antenna was studied with the aim of providing the author of this dissertation a way of developing a secondary project, so to complete the approach on patch antennas. To do so, the challenge was to study, optimize (in terms of physical dimensions and reflection coefficient magnitude) and evaluate the behaviour of the antenna portrayed in [30] in the vicinity of the human body. Throughout this section the requirements that make a patch antenna function in the UWB range are explored, and the impact of a CPW solution (instead of the microstrip one previously assessed) is analysed.

In section 3.1, the microstrip solution for patch antennas is referred and used for the construction of the dual-band antenna. This solution is seen in the following chapter to be of great importance, regarding the performance in the proximity of human limbs. However, for the sake of variety and to emphasize other solutions that are also commonly used, the CPW feeding employed in the antenna of

[30] is maintained. Also, the lack of a copper shield similar to the one employed in section 3.2 intrigued the author, and an opportunity to evaluate the robustness of microstrip and CPW solutions against the characteristics of human tissues presented itself.

But first, several attempts were tried until the author reached the final design. In [60] and [12], a comparison regarding the performance of the microstrip and CPW solutions is evaluated, and other variants of the latter are also suggested. Thus, the antenna went through different configurations until it reached its final format, as illustrated in Figure 3.22. Although only two approaches are portrayed, three were studied; the third one has the same configuration as Figure 3.22(a), but with a copper shield (with the same dimensions as the substrate) on the back, printed on the substrate. So basically, and with reference to UWB antennas, the conventional CPW solution was studied (Figure 3.22(a)), as well as the microstrip one (Figure 3.22(b)). The third solution is an alternative to the latter, denominated by Grounded Coplanar Waveguide (GCPW) [60] [12].

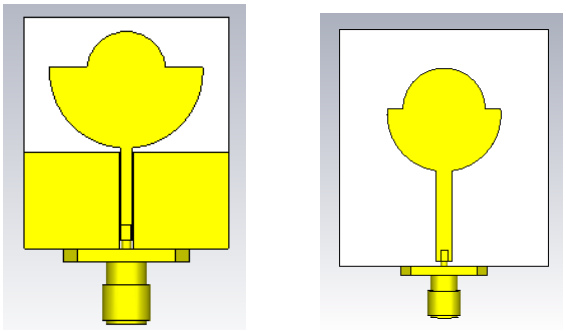

(a) CPW-fed UWB antenna with two square ground planes on either side of the center strip.

(b) Microstrip UWB antenna.

Figure 3.22: Feeding solutions for UWB antennas

The CPW solution is very attractive and is extensively used for wideband applications [60] [2]. It exhibits low dispersion, due to the small gap between the feeding line and the sided ground planes, bringing up again the desired little fringing fields mentioned hitherto. The GCPW solution will be further deepened, but it was studied as it consists in a mixture of the CPW and the microstrip solutions [1]. Despite the powerful isolation provided by having a signal conductor in between two ground planes, when compared to the conventional microstrip feeding the GCPW structure has the low dispersion of CPW-fed antennas, enduring small radiation losses, and has also the advantage of suffering little performance degradation at higher frequencies. However, the inherent architecture makes antennas that employ GCPW to be more sensitive to the physical fabrication techniques of the patch, making it a more suitable alternative for high-frequency applications.

With all the characteristics mentioned above, the designs were subjected to simulation and optimization using again the $CST^{TM} MicrowaveStudio$ software. The results are presented in Figure 3.23, and each arrangement was optimized using the $Optimizer$ tool incorporated in the simulation software, with the sole purpose of having antennas that work in the standard UWB band (frequency range from 3.1 GHz to 10.6 GHz) [18]). For the concerned design, it can be clearly seen that only the CPW-fed format

of Figure 3.23(a) almost satisfies the desired goal.

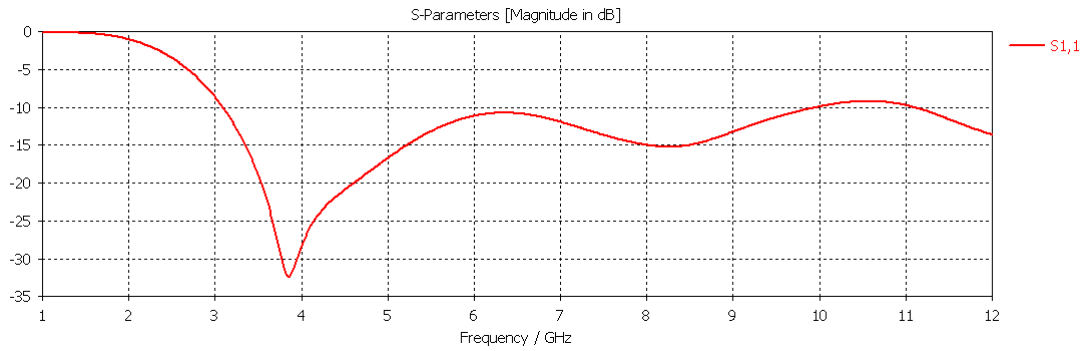

(a) $|S_{11}|$ parameter of the CPW-fed UWB antenna.

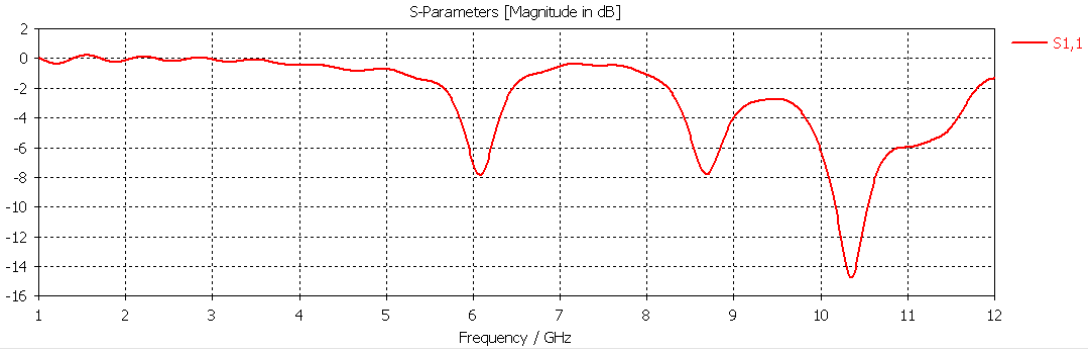

(b) $|S_{11}|$ parameter of the microstrip UWB antenna.

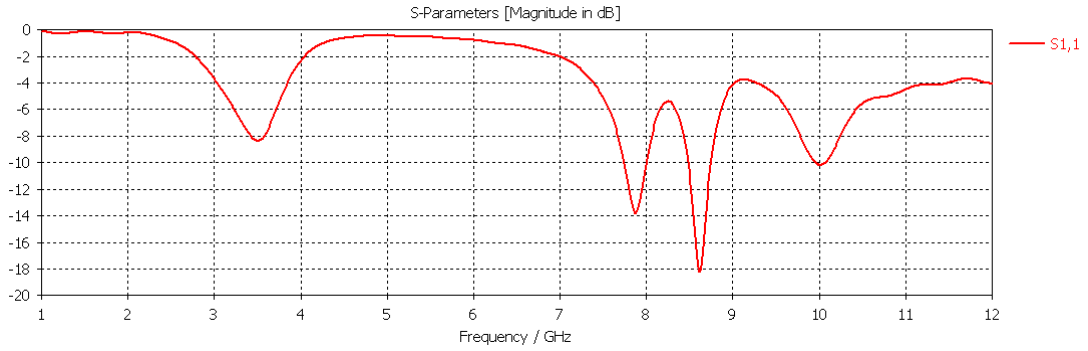

(c) $|S_{11}|$ parameter of the GCPW-fed UWB antenna.

Figure 3.23: $|S_{11}|$ parameters of different feeding configurations regarding UWB applications

With that in mind, the author carried on to improve both the $|S_{11}|$ parameter of the CPW UWB antenna and its physical dimensions. The design of the patch was kept, as the main goal was not to find a new CPW-fed UWB antenna, but to evaluate whether or not this architecture is suitable for wireless communications near the human body. Thus, attention was given to parameters that had a more noteworthy influence on the performance of the antenna, such as the dimensions of the center strip, the gap between the latter and the sided ground planes, and the gap between the ground planes and the bowl-shaped part of the patch (respectively represented in Table 3.3 by bw, i and k). Nevertheless, the other parameters were also optimized, so to obtain the best possible configuration.

The CPW-fed antenna, however, did not fully cover the standard UWB band (as one can observe from Figure 3.23(a), in which according to the $-10dB$ criteria only works approximately from 3.15 to

around 10 GHz.) The author of this dissertation then proceeded to follow the gist implied in [3], which is that the UWB response can be further enhanced by achieving a certain ground plane slot, size and/or shape. The introduction of slots was out of the envisioned objective, so resizing and reshaping was looked into. A parametric study involving the two ground planes was conducted, and the outcome is depicted in Figure 3.24(d). One can observe a slight improvement in the magnitude of the reflection coefficient when the shape of the ground planes goes from the square format (Figure 3.24(a)), passing by the elliptical one (Figure 3.24(b)), to the scenario in which each ground plane has a configuration of a quarter of a circumference (Figure 3.24(c)). In the last two situations the antennas fully cover the UWB range, and since the shape of the ground planes directly affect the $|S_{11}|$ parameter, the author decided to continue the study with the quarter-of-circumference case, as the elliptical ones showed unstable results when simulating for different bigger radii (meaning not fully covering the UWB range when the bigger radius suffers negligible deviations).

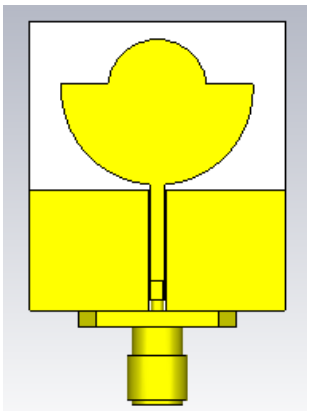

(a) CPW-fed UWB antenna with square ground planes.

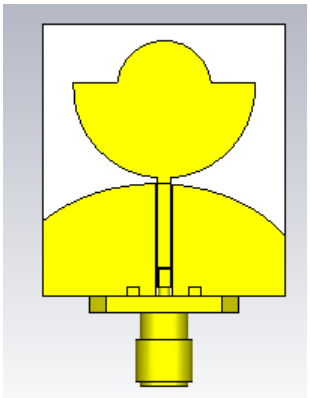

(b) CPW-fed UWB antenna with elliptical ground planes.

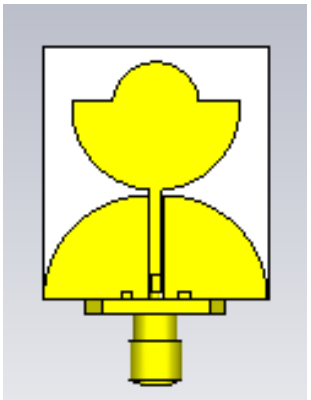

(c) CPW-fed UWB antenna with circular ground planes.

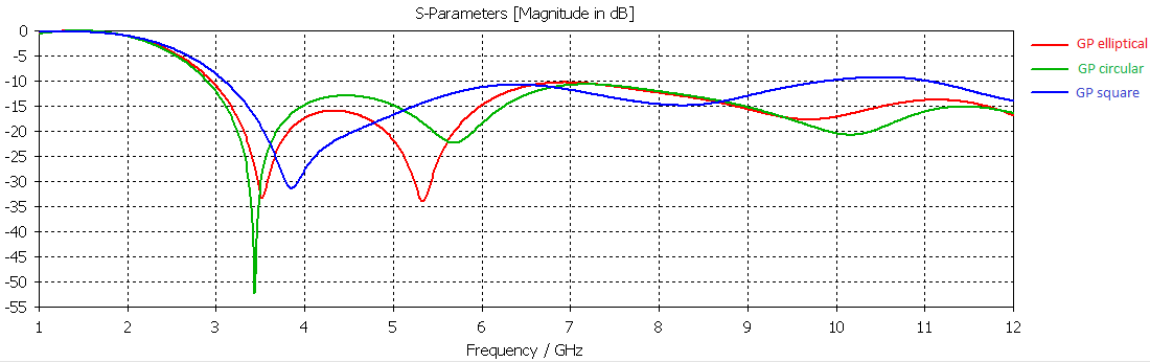

(d) $|S_{11}|$ parameters of different ground plane configurations regarding CPW-fed UWB applications.

Figure 3.24: Different ground plane configurations regarding CPW-fed UWB applications and their impact on the respective $|S_{11}|$ parameters.

Therefore, the final design of the UWB antenna optimized is presented in Figure 3.24(c), and Table 3.3 displaying the values, in mm, of the dimensions of Figure 3.25. This antenna is again printed photolithographically on $RogersRT/Duroid^{TM}5880$, with the same characteristics as previously mentioned: thickness h of 1.57 mm, relative permittivity ε_r of 2.2 and loss tangent $tan\delta$ of 0.0009. On top of the perks enumerated in section 3.1, the material reveals a thickness enough to broaden the bandwidth.

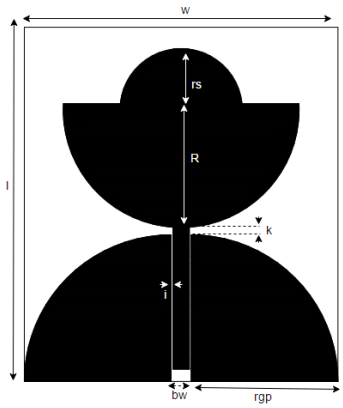

Figure 3.25: Geometry and design parameters of the optimized CPW-fed monopole antenna.

w	l	R	rs	bw	rgp	i	k
25.65	29	9.64	5	1.335	12	0.16	0.6

Table 3.3: Parameter values, in mm, of the antenna presented in Figure 3.24(c).

Chapter 4

Prototype test of the designed antennas

The increased interest and consequent investigation of BCWCs mentioned in the previous chapters has been focusing researchers in wearable devices, whether as a part of clothing or on the human user. However, the use of such devices near the human body have a completely different behaviour from when performing in free-space. One must take into account the human body interaction with them, and how their electromagnetic performances are affected, as many factors may degrade them. One particular cause that contribute to that deterioration is the influence of the electrical characteristics of the body tissues, which are thoroughly evaluated throughout this chapter. In Chapter 3 the whole process of designing a dual-band antenna and an UWB antenna was described, as well as the numerical evaluation of their main parameters. This chapter presents the main goal of this dissertation, which is the assessment of the behaviour of both antennas in the vicinity of the body of a human user. To do so, section 4.1 firstly fully characterizes the fabrication process. Sections 4.2 and 4.3 guide the reader through a detailed appraisal of the behaviour of the designed and developed dual-band and UWB antennas when put next to a human limb, respectively. That includes the comparison between the simulated and measured results in terms of the $|S_{11}|$ parameter, which is evaluated in a free-space scenario and in the vicinity of the human body. The latter is assessed by using simple four-layered models of a human arm in the CST software, and then comparing them when putting the antennas next to an actual human user. Each section also presents the calculation and inferred conclusion of the SAR parameter.

4.1 Fabrication and measurement setup

After the optimizations performed to the designed antennas of Chapter 3, the following step is to physically build and test them. Firstly, the layout of the antenna is exported from $CST^{TM} MicrowaveStudio$ to AutoCAD, a software application that provides a two-dimensional computer-aided design of the layout. The resultant production mask is converted to .pdf in the real scale (1:1 mm), as shown in Appendix B,

and printed.

In a second approach, the mask is photolitographically printed (with copper) on the substrate. The following procedure is called 'chemical etching', and consists on dissolving away (in a corrosive way) the parts that do not belong to the layout of the antennas. In order to do that, this fabrication method uses chemicals (entitled photoresists or etchants), and is then submitted to a whole process to minimize the effects of the surrounding environment on it. Firstly, the metal pattern is assiduously cleaned (for this case it was used a degreaser, then it was washed off, and then cleaned one second time with an acid wash), so to ensure it is free from detritus or other impurities that may disrupt the process. After being dried, the patch is submitted to a piece of machinery that lights both sides (front and back) with an ultraviolet (UV) sensitive photoresist. Although a negative photoresist is usually employed in metal etching, in this case a positive one was used. The former is usually utilized because it polymerizes when the UV light incises on it, allowing the unexposed metal portions to be etched away and protecting the desired metal layout underneath against dissolution [15], while the latter does the exact opposite (basically, the portion of the positive photoresist that is exposed to the UV light becomes soluble and are dissolved away). The positive resist was employed due to the sensitivity of negative resists to the swelling phenomena, which occurs when the developer solution penetrates into the photoresist material, resulting in a distortion of the desired layout [27].

The next step of this fabrication method is to put on each side of the patch an image of the metal pattern. This allows for separating the parts that are meant for dissolution from the ones that correspond to the metal pattern. After that, the patch goes to a controlled environment, with exposure to UV light, so to harden the pattern. The unexposed parts of the photoresist are washed away, and the remaining goes under the etching part of the chemical etching process. Both sides are sprayed with a specific acid that etches away the portions that were not subjected to the UV light, leaving nothing else but the pretended pattern. The patch finally undergoes a proper alkaline solution to wash away the rest of the photoresist and the cleaning process of the beginning is again performed.

The final format is inspected under an adequate microscope, and sometimes the process is not 100$\%$ accurate, resulting in microscopic parts that are not filled with the metal. However, that may be achieved with a correcting pen. For this dissertation the chemical etching was the only option available. Other more accurate fabrication methods can be used, one of them consisting in using an inkjet printer (more detailed information can be found in [4]).

After the chemical etching process, the antennas are ready for testing. The measurements were performed in the RF Laboratory at Instituto Superior Técnico. A Vector Network Analyzer (VNA) $E5071C$ from Agilent Technologies, represented in Figure 4.1(a), was employed to carry them, and was firstly calibrated and defined to a frequency range that was suitable for the work (see Figures4.1(c) and 4.1(d)). A RF cable was directly connect to the feed line of the antenna, via the connector, as shown in Figure 4.1(b).

The following sections are dedicated to the evaluation of the behaviour of both antennas, in free-space and in the vicinity of the human body. Conclusions are drawn considering the comparison between the simulated and measured results, with respect to the mentioned scenarios.

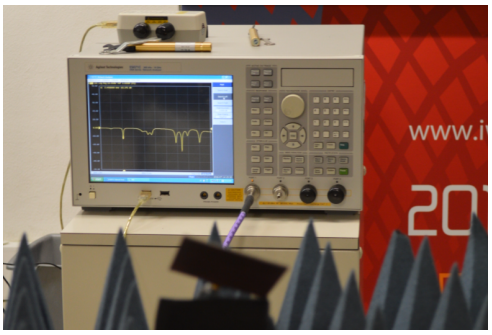

(a) VNA.

(b) Measurement setup of the dual-band antenna.

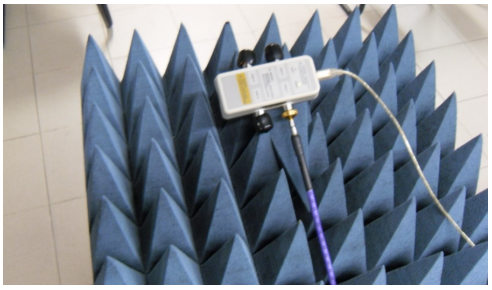

(c) VNA automatic calibration process.

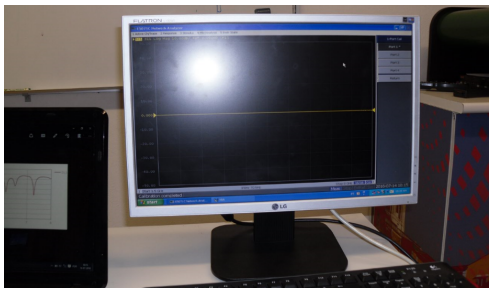

(d) Calibration completed.

Figure 4.1: Measurement setup for the dual-band antenna.

Frequency [GHz]	Impedance Bandwidth [MHz]	Percent Bandwidth [%]	f_1 [GHz]	f_2 [GHz]
2.45	24.2	0.99	2.4369	2.4611
5.8	89.6	1.54	5.7697	5.8593

Table 4.1: Measured results for the impedance and percent bandwidth of the dual-band antenna designed.

4.2 Dual-band Antenna

4.2.1 Free-space scenario

In this section, the simulated and measured results regarding a free-space scenario are compared. Figure 4.2 shows the outcome of the laboratory measures (see Figure 4.2(a)) and the comparison with the simulated return loss (Figure 4.2(b)). A fitting agreement is achieved, with the visible differences being a decrease in amplitude and in bandwidth, and a slight frequency shift.

Although the antenna does not fully cover the ISM bands of 2.45 and 5.8 GHz, as it can be seen in Figure 4.3, it still works in both ISM bands, according to the $-10dB$ criteria referred in section 2.3.1. Figures 4.3(a) and 4.3(b) depict the operating bands.

Applying equation 3.11 from subsection 3.2.1, and designating again f_2 and f_1 as the higher and lower frequency limits of the operating bands, respectively, the measured impedance and percent bandwidth are expressed in Table 4.1. One can see how narrow both frequency bands are, by having such small percent bandwidths.

In this section, the dual-band antenna was assessed in free-space. The results were the expected

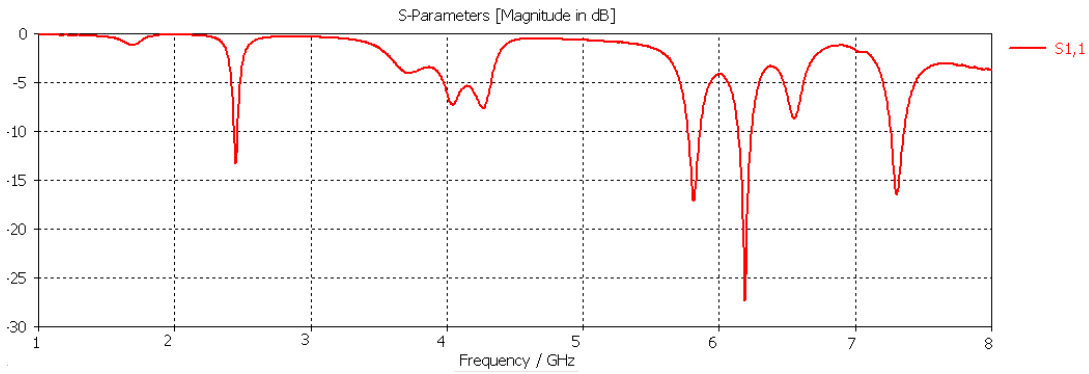

(a) Measured $|S_{11}|$ parameter.

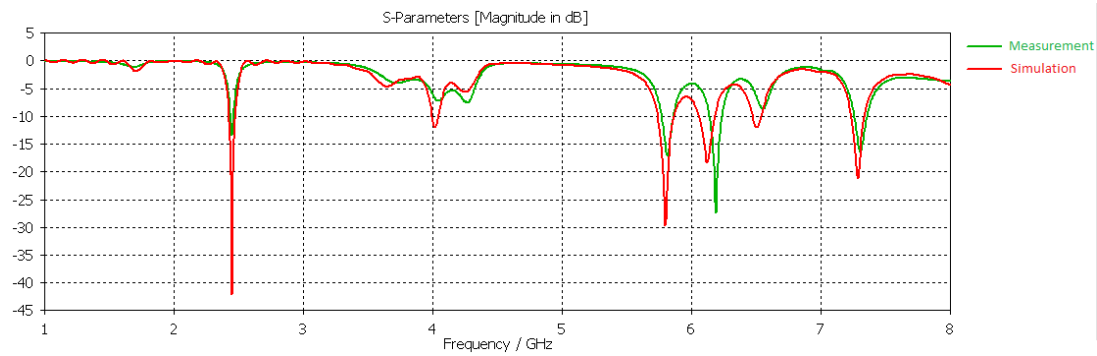

(b) Measured and simulated $|S_{11}|$ parameters.

Figure 4.2: Return loss of the dual-band antenna in free-space.

ones and from Figure 4.2(b), one can evidence the robustness of the antenna designed. The slight differences may occur from several factors, such as the influence of the RF cable (see Figure 4.1(b), which is translated into current leakage and electromagnetic scattering [46].

SAR

In this subsection, the SAR parameter of the developed dual-band antenna is fully characterized and determined, so to meet the limits defined by the International Commission on Non-Ionizing Radiation Protection (ICNIRP) to the exposure to time-varying electromagnetic fields citesar. This is an important matter, since in this dissertation the antennas designed are to operate at a few GHz, and exposure to electromagnetic fields at frequencies above 100 kHz can lead to a great deal of energy absorbed by the human body, and its consequent temperature rise. This vulnerability can produce adverse health effects, so the entity ICNIRP established guidelines for restricting the electromagnetic exposure and produce an adequate level of protection to it.

The specific absorption rate thus translates into a number the power absorbed (or dissipated) per human body tissue, when exposed to electromagnetic waves [7]:

$$SAR = \frac{\sigma E^2}{2\rho}. \tag{4.1}$$

The conductivity of human tissue is σ (given in $S.m^{-1}$); ρ is the density of the tissue sample (in

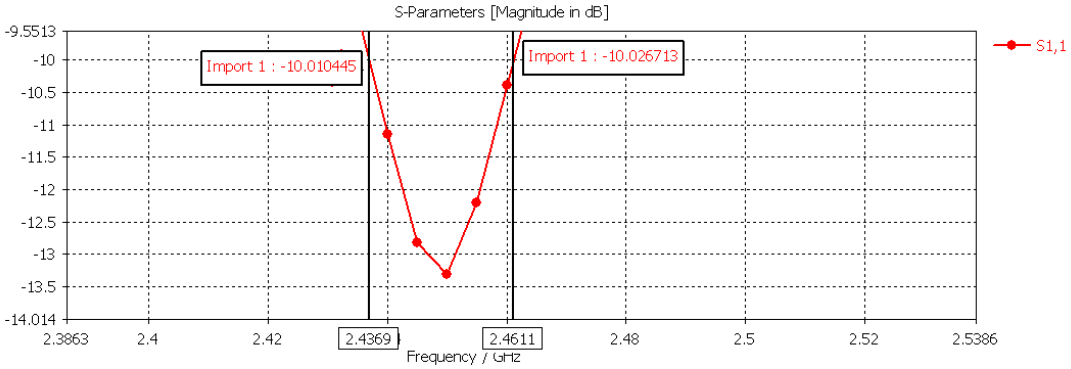

(a) Zoom in at 2.45 GHz.

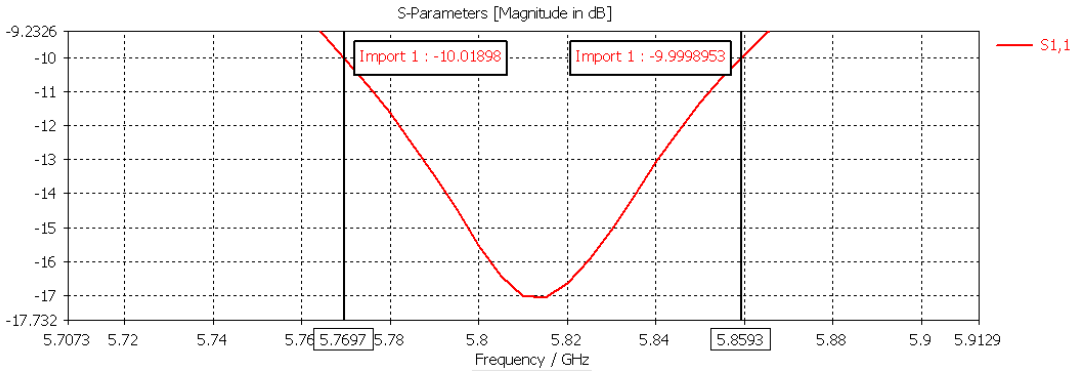

(b) Zoom in at 5.8 GHz.

Figure 4.3: Return loss of the dual-band antenna in free-space.

Exposure characteristics	Frequency range	Whole-body average SAR ($W.kg^{-1}$)	Localized SAR (head and trunk)($W.kg^{-1}$)	Localized SAR (limbs)($W.kg^{-1}$
Occupational exposure	10 MHz to 10 GHz	0.4	10	20
General public exposure	10 MHz to 10 GHz	0.08	2	4

Table 4.2: Basic restrictions for time varying electromagnetic fields for frequencies up to 10 GHz.

$kg.m^{-3}$), and E is the internal electric field strength (in $V.m^{-1}$). The SAR values come in watts per kilogram ($W.kg^{-1}$), according to the International System (IS).

Before proceeding to the calculation of the SAR, by using the CST software, Table 4.2 summarizes table 4 of [20] for the present case of the dual-band antenna. It shows reference levels, obtained through mathematical modelling and extrapolation from laboratory result investigations at specific frequency ranges. These values are presented as maximum ones, so they should not surpass them, as it can then be hazardous to the human health, and consider an averaging mass of 10 g of contiguous human body tissue.

Being the difference between occupational exposure and general public exposure the fact that the former refers to the exposure experienced by an individual at his/hers workplace and the latter the exposure faced by future users (members of the general public), the aimed SAR limit for this dissertation is the smallest one that applies to human limbs: the $4W.kg^{-1}$. Bearing this in mind, one can finally proceed

Frequency [GHz]	Tissue Mass [g]	Maximum SAR ($W.kg^{-1}$)	Total SAR ($W.kg^{-1}$)	Average power ($W.mm^{-3}$
2.45	10	5.1e-4	1.3e-4	1.7e-10
5.8	10	11.0e-4	1.9e-4	2.3e-10

Table 4.3: Simulated results for the Maximum SAR, Total SAR and Average power for 10 g of contiguous tissue, considering a distance between the dual-band antenna and the flat model of 3 mm.

Frequency [GHz]	Tissue Mass [g]	Maximum SAR ($W.kg^{-1}$)	Total SAR ($W.kg^{-1}$)	Average power ($W.mm^{-3}$
2.45	10	3.6e-4	1.0e-4	1.3e-10
5.8	10	7.8e-4	1.5e-4	1.9e-10

Table 4.4: Simulated results for the Maximum SAR, Total SAR and Average power for 10 g of contiguous tissue, considering a distance between the dual-band antenna and the flat model of 7 mm.

to the calculation of the SAR parameter. This calculation takes place in the $CST^{TM} MicrowaveStudio$ environment, with the antenna placed 3 and 7 mm apart from the simple model of the human body. The one employed was the flat one, due to its simplicity and subsequent saving of computational time. According to the parameters of the tissues of the models (see Table 4.6), the total mass defined for the flat model equals 820 g. The SAR is frequency dependent, and is thus calculated for the wanted working frequencies. With an input power normalized to $1mW$ for all the simulations, Tables 4.3 and 4.4 show the results obtained with the most relevant parameters that compose the SAR calculation, for the cases in which the antenna is distanced from the flat model by 3 and 7 mm, respectively.

The most important criterion that one has to compare is the Maximum SAR value. Table 4.2 shows the limit established by ICNIRP is $4W.kg^{-1}$. As one can see, the values obtained are considerably lower than this limit, and that comfortable margin permits the user to not worry about radiation absorption. To also note that, as the distance grows, the SAR values diminish, which is an expected conclusion (the bigger the distance the lesser the radiation absorption). The antenna shows as well an increase of the absorption in the higher frequencies, also expected from Equation 4.1.

The calculated SAR values on this subsection are way below the maximum values allowed by ICNIRP. The dual-band antenna can therefore be tested on a human user with no concerns.

4.2.2 Behaviour in the vicinity of the human body

This section presents the simulated results obtained in $CST^{TM} MicrowaveStudio$ regarding the human body influence on the performance of the antenna. As it has been identified before, the tissues of human limbs are heavy absorbers of electromagnetic waves, which can harshly alter the main parameter at study: the impedance bandwidth of the antennas. For that, the models that were previously introduced in section 2.2.1 and detailed in [30] are employed in this study, and are seen as accurate enough so to evaluate the performance of the antenna when fixed on a human arm (in this thesis the experiments are conducted on the arm of a human user, as it is a favourable place to place the antenna). Figures 4.4(a) and 4.4(b) show the simulation scenario, making use of the flat and elliptical simplified models of a human limb, respectively.

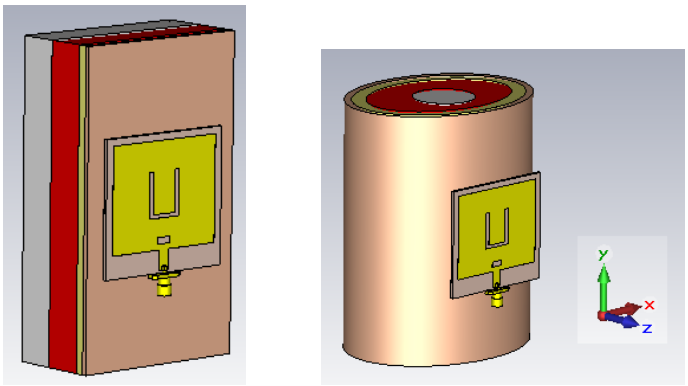

(a) Flat model. (b) Elliptical model.

Figure 4.4: Simplified models used for simulation.

Tissue	Skin (dry)	Fat	Muscle	Bone (cortical)
Thickness (mm)	2	4	17.5	17.5

Table 4.5: Thickness of the selected human body tissues.

In this work, the voxel models mentioned in section 2.2 will not be used, which are complex and take too much computational time. Also, it would be impossible to compare the simulation results with a real phantom, as it could not be simply built. Instead, the simplified models illustrated in Figure 4.4 are used, and turn out to be accurate enough to predict the behaviour of the designed antennas in the vicinity of the human body, as it will be further seen.

As the human body is a heterogeneous multi-layered medium, both models comprise the four main tissue layers that have the most influence in the performance of antennas: skin (dry), fat, muscle and bone (cortical). For an accurate modelling, the primary dielectric attributes of the tissues were retrieved from [21], an online tool that determines the dielectric properties of body tissues in a frequency range from 10 Hz to 100 GHz. More precisely, the 'Text-mode, on-line web application', which allows the user to select the desired frequency range for a single tissue and print the requested parameters (permittivity and loss tangent). These 'new' materials are added to $CST^{TM} MicrowaveStudio$, and take into account the dispersion characterization of each tissue, as can be seen in Figure 4.5. So instead of having fixed values for the relative permittivity and the loss tangent of each tissue, they are discriminated depending on the frequency, and thus numerical instability errors may be avoided [29].

The dimensions of each model are indicated in Table 4.5. The simple versions of a human arm are of 140 mm length and 82 mm width (values long enough to fully subject the antenna to the electromagnetic interference of the tissues), with the same thickness. To note that the models were designed according to [30] and [29]; the bone is deviated 4 mm from the center in the elliptical model, and both models use the same thickness. Table 4.6 enumerates the characteristics of the relevant tissues (meaning the ones selected, because tissues with a permittivity lower than the one of the bone have negligible influence on the impedance bandwidth of the antenna), in terms of their densities, in order to further define and assess the SAR parameter.

Next, and since in subsection 4.2.1 it was already seen that there is no problem in doing that, regard-

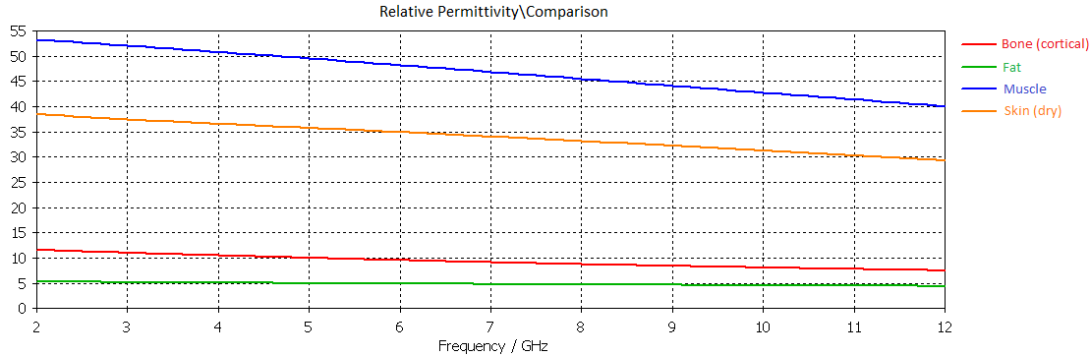

(a) Relative permittivity.

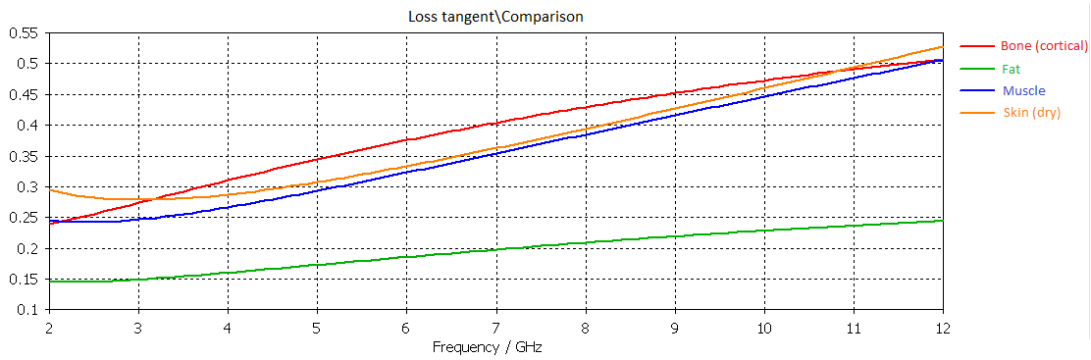

(b) Loss tangent.

Figure 4.5: Electric properties of the tissues that compose the simplified models of the human body.

Tissue	Skin (dry)	Fat	Muscle	Bone (cortical)
Density ($kg.m^{-3}$)	1100	919.6	1060	1500

Table 4.6: Density of human body tissues.

ing the SAR parameter, the dual-band antenna was tested on the arm of a human user (in this case, the author himself). To do so, a latex band was used to clinch the antenna on the arm (see Figure 4.6(a), as well as a strip of polyethylene, so to help simulating specific distances between the antenna and the arm (3 and 7 mm), as one can observe in Figure 4.6(b).

The measured results are portrayed in Figure 4.7. It shows the comparison between the simulated free-space case and the one obtained in laboratory, and it also includes the experimental results retrieved when the antenna was put right next to the human arm of the user (0 mm case); when it was distanced by 3 mm (again, with the help of the arrangement of Figure 4.6(b)), and when the distance increased to 7 mm. It is clear now that, apart from slight changes in the $|S_{11}|$ parameter that were earlier acknowledged in section 4.2.1, the antenna is strong against the presence of the human body.

Another goal of this evaluation consists in showing how the simple models are accurate enough to predict the behaviour of antennas. Figure 4.8 offers the comparison between the simulated results (using the elliptical and the flat models) and the measured ones, for the case of when the antenna is fixed on the human arm (0 mm case). It shows an excellent agreement between the simulated and measured results, and thus should be employed when simulating these types of antennas, as it allows the user to save time in the computational process. Also, since from Figures 4.4 and 4.8 one can observe that, although they

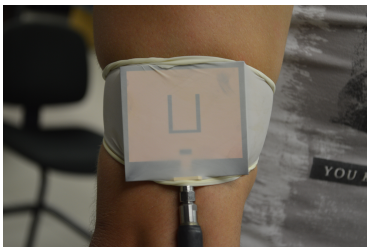

(a) Antenna measured on the arm of the human user.

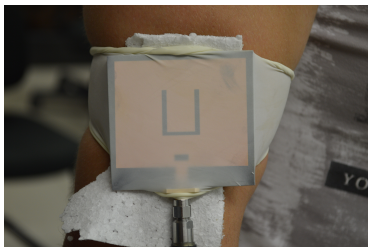

(b) Strip pf polyethylene used to specify a distance between the antenna and the human user.

Figure 4.6: Measurement setup of the dual-band antenna, supported by a small latex band and employing polyethylene.

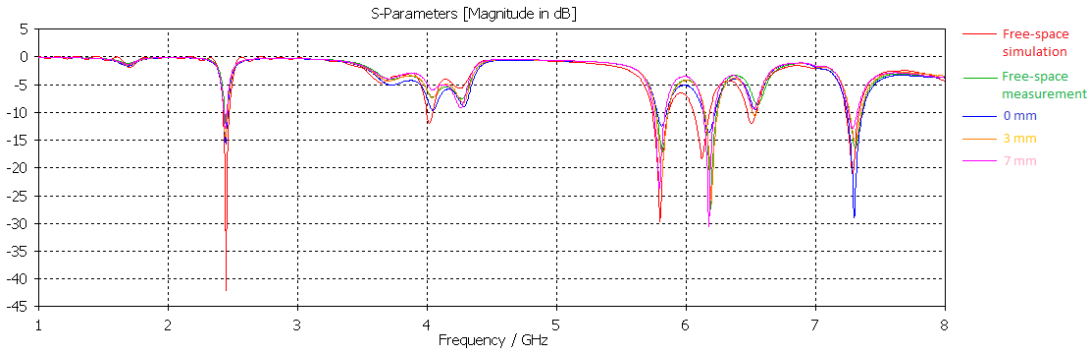

Figure 4.7: Comparison between the simulated and measured return losses for the cases of free-space and when next to the human body.

are very similar, the flat model is the one that best fits the measured results comparing to the elliptical model. Since CST utilises the Finite Integration Technique (FIT), the electromagnetic computation is much faster if square/rectangular shapes are simulated [9], and the flat model is therefore the one to use (as a quick and reliable term of evaluation).

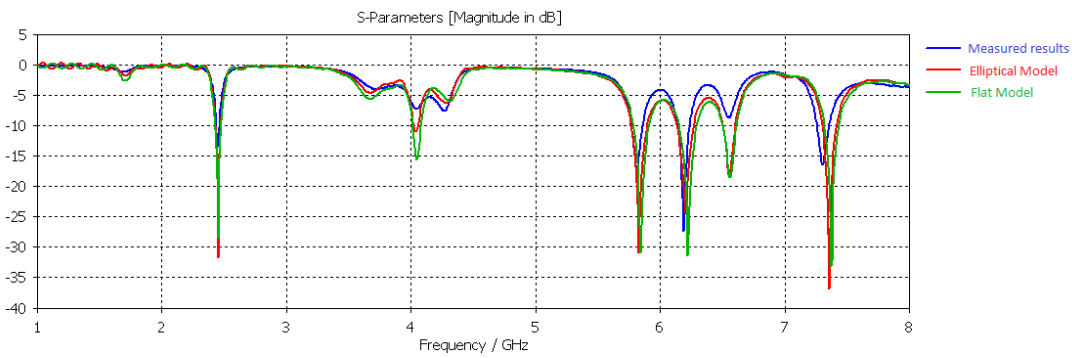

Figure 4.8: Prediction of the behaviour of the antennas in the vicinity of the human body by using simple models of human limbs.

4.3 UWB antenna

In this section, the procedure conducted in sections 4.2.1 and 4.2.2 is applied to the designed UWB antenna. The simulated and measured results regarding the performance of the UWB antenna are evaluated, in terms of the $|S_{11}|$ parameter. The experiments are conducted in two different scenarios: free-space and in the vicinity of the human body. For the first one, the antenna is seen to cover the optimized communication standard UWB range only if reflections of around $20\ 25\%$ of the power fed to the antenna are tolerable. For the second case, the antenna is simulated using simple models of a human arm, followed by its measurements near an actual arm of a human user. Although the distance between the arm surface and the antenna (0, 3 and 7 mm), so to enforce the correlation between the free-space case results, none was found; solely that the antenna, with the present configuration, is not robust enough to be used for near-the-human-body functions.

4.3.1 Free-space behaviour

In this subsection, the simulated and measured results regarding a free-space scenario are compared. Figure 4.9 shows how the antenna was mounted and measured in the laboratory. Figure 4.10 shows the outcome of the experimental measures and compares it with the simulated return loss. As one can observe from the measured data, the antenna presents an up-shift from around 2.9 GHz to approximately 4.9 GHz in the lower -10 dB frequency edge. Several factors can be associated to this performance degradation, amongst them the possible errors in the fabrication process (such as the low mechanical resolution of the cutter, meaning that the substrate was cut with the best precision one can get by simultaneously using the hands to hold the antenna and the eyesight to know where to cut). The impedance detuning and consequent decrease in the impedance bandwidth represents a violation of the $-10dB$ criteria, and thus the antenna does not cover the targeted 3.1-10.6 GHz UWB standard. However, depending on the aimed application for this antenna, one can appeal to the $-6dB$ criteria (which is verified in Figure 4.10). If so, the UWB standard is clearly covered and the antenna satisfies the main performance requirements.

Figure 4.9: Measurements in free-space for the UWB antenna.

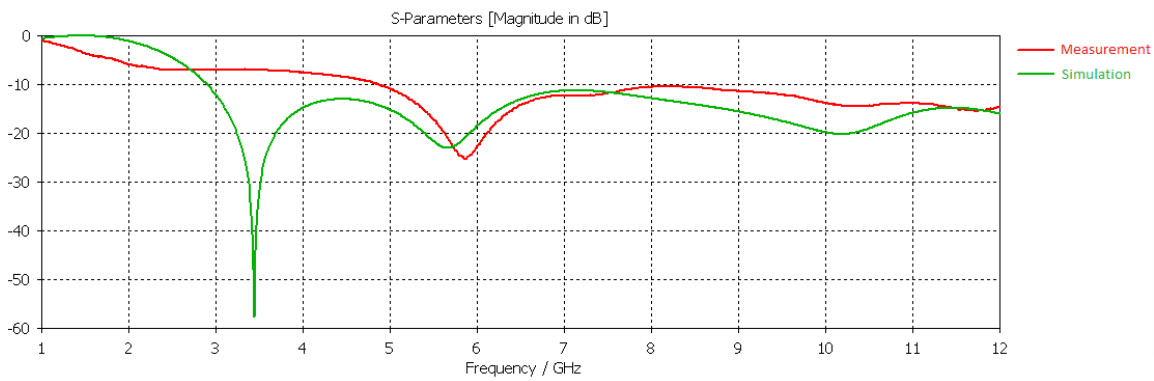

Figure 4.10: Comparison between the measured and simulated $|S_{11}|$ parameters for the UWB antenna.

Frequency [GHz]	Tissue Mass [g]	Maximum SAR ($W.kg^{-1}$)	Total SAR ($W.kg^{-1}$)	Average power ($W.mm^{-3}$
3.1	10	0.02	1.49e-3	1.84e-9
6.85	10	9.82e-3	3.62e-4	4.47e-10
10.6	10	0.01	4.66e-4	5.76e-10

Table 4.7: Simulated results for the Maximum SAR, Total SAR and Average power for 10 g of contiguous tissue, considering a distance between the UWB antenna and the flat model of 3 mm.

SAR

In this subsection the SAR values for the designed UWB antenna are presented. It follows the exact same procedure of subsection 4.2.1, as frequencies above 100 kHz are dealt with, so Table 4.2 is still valid and therefore the maximum values ought to be respected. Three different frequencies were chosen to perform the quantification of the SAR parameter: the starting frequency of a standard UWB antenna (3.1 GHz), the ending one (10.6 GHz), and the one that is in-between those two (6.85 GHz). The input power was once again normalized to 1 mW, as it was the power fed to the antenna during the measurements. The flat model is employed, weighing a total mass of 820 g. Tables 4.7 and 4.8 show the results obtained with the most relevant parameters that compose the SAR calculation, for the cases in which the antenna is distanced from the flat model by 3 and 7 mm, respectively.

The aimed SAR limit for this antenna is still the Maximum SAR value of $4W.kg^{-1}$. Once again the values obtained are considerably lower than this limit (highest value of 0.0234159 for the 3 mm distance case and 0.0198671 for the 7 mm one). The antenna is thus prepared to be used in the vicinity of the human body with no restrains.

Frequency [GHz]	Tissue Mass [g]	Maximum SAR ($W.kg^{-1}$)	Total SAR ($W.kg^{-1}$)	Average power ($W.mm^{-3}$
3.1	10	0.02	1.27e-3	1.57e-9
6.85	10	3.17e-3	1.23e-4	1.52e-10
10.6	10	3.94e-3	2.58e-4	3.19e-10

Table 4.8: Simulated results for the Maximum SAR, Total SAR and Average power for 10 g of contiguous tissue, considering a distance between the UWB antenna and the flat model of 7 mm.

4.3.2 Behaviour in the human arm proximity

In this subsection, the evaluation of the behaviour of the constructed UWB antenna near a human arm takes place. The simple models employed in section 2.2.1 are once again used, with the characteristics previously detailed in Figure 4.5 and Tables 4.5 and 4.6, as one can observe from Figure 4.11, to simulate the performance of the antenna near the human body.

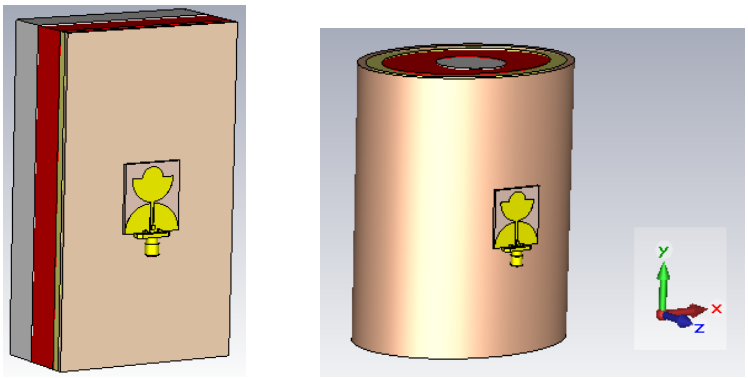

(a) Flat model. (b) Elliptical model.

Figure 4.11: Simplified models used for simulation of the UWB antenna.

The results of the simulation using $CSTMicrowaveStudio$ are portrayed in Figure 4.12. It is noteworthy the strong influence of the tissues of the simple models on the performance of the antenna. For the established goals for this antenna, the one that best suits the project is the elliptical one. It shows the antenna does not work from around 4.2 to 5.5 GHz, whereas the flat one decreases the magnitude more significantly, breaching the $-10dB$ limit from approximately 5 to 7.8 GHz. Still, both models do not cross the $-6dB$ boundary, and depending on the envisioned applications for this antenna they can still be feasible.

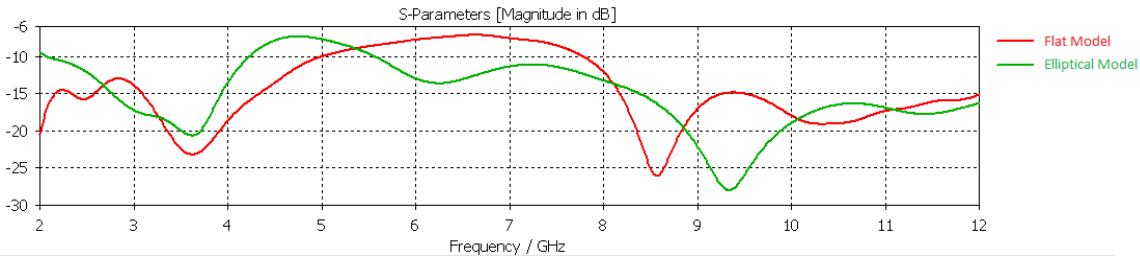

Figure 4.12: Influence of the simple models on the $|S_{11}|$ parameter of the UWB antenna.

However, a comparison with real life conditions is fundamental to consolidate the apparent conclusions regarding the effects of the human body on the impedance matching of the UWB antenna. To do so, the same procedure of section 4.1 and subsection 4.2.2 is followed. The antenna is placed on the arm of the human user and fixed with a latex band (see Figure 4.13(a)). To keep the antenna at a certain distance of the human arm, a strip of polyethylene is again employed (Figure 4.13(b)). The whole setup from Figure 4.13 was measured with the same material, the VNA E5071C, from Agilent Technologies.

The results obtained in laboratory are illustrated in Figure 4.14, and are also compared to the simulated and measured free-space case. By comparing with Figure 4.12 one can notice that the elliptical

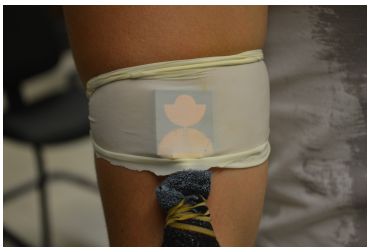

(a) Antenna measured on the arm of the human user.

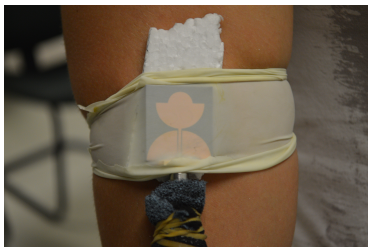

(b) Strip of polyethylene used to specify a distance between the antenna and the human user.

Figure 4.13: Measurement setup of the UWB antenna, supported by a small latex band and employing polyethylene.

model does in fact best approach the measured results for the 0 mm case, but only when compared to the flat one. The presence of the arm of the human user severely affects the operation band of the designed UWB antenna, and it is observed that the lower resonance frequency is down-shifted from 3.6 to 2.1 GHz, and the higher one is also down-shifted from 9.3 to 6.8 GHz.

With respect to the 3 and 7 mm cases, the correspondent resonance frequencies suffer both an up-shift and a drastic decrement on their magnitudes, which is more conspicuous in the lower frequencies. In the higher frequencies the reflection coefficient appears to endure smaller cuts in the magnitude, and thus stay quite stable, regarding antenna matching. This observation is congruent with the one from section 3.3, evidencing one of the advantages to the CPW feeding, which is a higher resistance to performance degradation at higher frequencies. Nevertheless, the farther the distance between the antenna and the human limb, the more the results resemble the free-space case, although it is not as noticeable as in the case of the dual-band antenna.

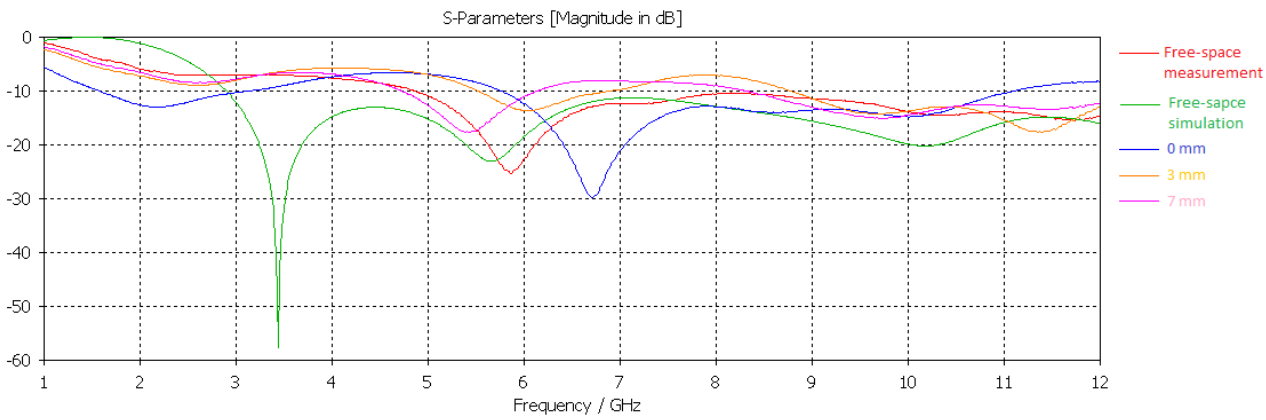

Figure 4.14: Comparison between the measured $|S_{11}|$ parameter for different distances of body proximity.

Although several factors may contribute to the deterioration of the performance of the CPW-fed UWB antenna built, such as the feeding cable effect for such a small antenna or the difference between simulating an antenna and measuring it in real conditions, the results are the expected ones. In order to be used on the human body, the antenna needs a better electromagnetic shielding. Comparing to the microstrip antenna designed previously evaluated in this chapter, one can observe the sensitivity of the

CPW solution to the proximity of the human body. As an example, in [2] and [37] are presented UWB antennas that employ the microstrip solution, revealing better robustness against the characteristics of the human tissues. Notwithstanding, the CPW feeding structure was chosen due to its reduced complexity and easy integration into wearable devices, which is very attractive for future work with these antennas.

Chapter 5

Conclusions and Future Work

In this chapter, the main conclusions of the dissertation are presented and summarized. The first part briefs what was studied and what was achieved. The second part offers proposals for future work with the antennas developed.

5.1 Conclusions

Nowadays there has been a growing interest in body-centric wireless communication systems, due to its vast range of applications, whether it is for military utilization, medical operations or even for entertainment-related functions. An imperative element of those systems are the antennas, which are the components that support the communication between a device on the user and the off-body equipment. Therefore, the correct design of antennas for WBANs are crucial, not only due to the constant growth on traffic demands, but also because of the intense influence of the electromagnetic properties of the human body on the performance of these antennas.

On that note, the main purpose of this dissertation is to develop a robust microstrip-fed dual-band antenna that works in the ISM bands of 2.45 and 5.8 GHz and is to be used in the vicinity of the human body. The adjective 'robust' is meant both for a mechanically strong and electromagnetic interference-quasi-free antenna. In order to deepen that study, the dual-band antenna is designed and simulated using the $CSTMicrowaveStudio$ software, followed by its physical construction. As a secondary project, and so to expand to other types of antennas, the author reviews the CPW-fed UWB antenna produced in [30], and proceeds to optimize the antenna (so to minimize its dimensions), followed by its study on a human user. The whole process that involved the design and optimization of both antennas is fully detailed, as well as the several scenarios where they were simulated, whether it was in free-space or on-body.

The dissertation is divided into five chapters, being the last one the present one. The first one introduces the theme and enumerates the goals to be achieved throughout the study, as well as what motivates the subject and its importance and contribute to the technological world. Chapter 2 focuses on the state of the art of antennas that are meant to be used in the vicinity of the human body. It introduces

the concept of BCWCs, and the main threat faced by these systems nowadays. It is highlighted the interaction between the antennas and the human body as the main challenge, and it is seen that the antennas must be small, compact and robust to de-tuning and performance degradation, in order to withstand that influence. Next, models of the human body are investigated. These are seen to be of quite importance, as they allow the developer of the antennas not only to evaluate their behaviour in a simulation environment, but also to ensure that they are under the limits of the SAR parameter established by the ICNIRP entity, in order to limit the exposure to time-varying electromagnetic fields and provide a healthy interaction with the user. These models, denominated as phantoms, are reviewed, and the author presents simple structures, as well as more complex ones. It is seen that the more complex ones require a certain type of materials that are not reachable to everyone, and take too much computational time. As an alternative, simple models of the human body can be used, and are found to be a quite accurate solution if one wants to predict the behaviour of the antennas in the presence of a human body.

In the remaining of the chapter, wearable antennas are reviewed, as in antennas that can be actually worn by the user, as well as the main challenges faced by them. It is seen that there are many aspects that must be considered when designing a wearable antenna, whether it is an accessory or textile antennas, and thus they are not as much attractive as a conventional antenna. Also, the emphasis of conventional antennas is in their general low cost and simple fabrication, which is a great factor for a more profound investigation on them, in terms of their future applications and commercial purpose. The state of the art of antennas that fulfil those requirements and are to be used on-body and communicate with devices off-body is presented next, providing the reader with some solutions that are displayed in the literature, as a way of directing the attention to single-band, dual-band and UWB patch antennas. An example of a single-band is presented, as that concept was immensely studied by the author, in order to understand the mechanics of a patch antenna and its electromagnetic behaviour response to alterations in their physical structure. The proposed dual-band served as an inspiration to produce the developed antenna. It revealed the author the importance of introducing well-positioned slots in the patch, as a way of inducing the appearance of a second resonance frequency (and more, if more slots are introduced). Finally, an UWB antenna is introduced. UWB technology is presently seen as an attractive solution for WBAN, as it allows for dimensioning smaller patch antennas and transmit high data rates over short distances, among other benefits. Here, not only it was the example that led the author to deepen his study on UWB antennas, but also one of the articles in the literature that point out the accuracy of simple models. Two simple models are designed (a flat and an elliptical one) and it is concluded that the use of a simplified elliptical model of a human arm is perfectly capable of predicting the performance of the antenna in the proximity of a human user, and is thus suitable for designing antennas for WBAN applications.

Chapter 3 guides the reader through the whole design, optimization and simulation process. The microstrip-fed solution is chosen to be utilized, due to the fulfilment of a priori specifications, such as their low cost, low profile, light weight, flexibility in terms of electromagnetic parameters, ease of fabrication and conformability to planar and non-planar surfaces, crucial for building a robust antenna for WBAN

applications. The concept is therefore thoroughly summarized, followed by the design of the desired antennas. All the details that drove the author to the final solutions are presented, from the most basic requirements, such as choosing the substrate, to the optimization of the several major parameters of the antenna that can have a great influence on its performance. The $RogersRT/Duroid^{TM}5880$ was chosen due to its inherent properties: its cost-effectiveness, its ability to overcome certain limitations imposed by the microstrip solution and the mechanical resistance it offers due to its thickness of 1.57 mm, among other factors. The author then proceeds to try and reach the main goal. Several attempts are presented, and conclusions are drawn from that. It is seen that, in order to properly operate when on a human body, the antennas must have a low front-to-back ratio; this is achieved by shielding the backside of the patch antenna, meaning covering that part with copper (chosen default conductive metal). Other problems, such as making the antenna radiate away from the body, is resolved with both the low permittivity of the substrate material employed and the configuration of inserted slots, that optimized the radiation in the pretended direction. The operation at the ISM bands of 2.45 and 5.8 GHz is achieved with the strategic insertion of a line-slot and an U-slot. The outcome is therefore a highly-efficient robust dual narrow-band antenna, small enough to be easily integrated with other microwave circuits and minimize surface wave propagation, with the proper radiation pattern pretended and a clear margin for operating at the wanted frequencies (in terms of its return loss).

The UWB antenna from [30] is here designed as a way of providing the author with a secondary case study, an antenna with a different operating frequency range and with a different feeding solution, the CPW one. The main concern for the design of this antenna is regarding its appropriateness for wireless communications near the human body, so the parameters that are given more attention are the return loss and the diminishment of the physical dimensions. A comparison between the microstrip solution and the CPW one is carried, and it is seen that the coplanar feeding has properties that are very attractive for wideband applications, such as its inherent low dispersion (translated into small radiation losses and thus higher efficiency) and little performance degradation at higher frequencies, among others. However, two factors worried the author: the lack of a copper shield on the backside of the CPW-fed antenna and features that are favoured in the microstrip solution, but not on the coplanar one. Hence, a few solutions are perceived, being the GCPW one the bast candidate. However, it is demonstrated that this solution is much more suitable for higher frequency applications, so the author proceeded to improve the antenna performance with the help of optimizing tools from CST. The final format is achieved through the resizing and reshaping of the ground planes, which lead to an UWB antenna with a quarter-of-a-circumference ground plane shape that fully covers the standard UWB range (according to the ITU Radio Regulations [24] and the $-10dB$ criteria), in terms of simulation.

Chapter 4 reveals the outcome of the whole process, comparing the simulated with the measured results. Firstly the author briefs the reader on the fabrication process and measurement setup. A calibrated VNA, from Agilent Technologies, is used for measuring purposes, and a RF cable is connected to the feed line of the antennas. After, the antennas are evaluated both in free-space and in an on-body scenario. In terms of simulation, two simple four-layered models of the human body are employed, one flat and one elliptical. In both antennas it is observed that the simple models can accurately predict the

behaviour of the antennas when in presence of a human user, and that both SAR values are way under the maximum value stipulated by ICNIRP. Regarding the dual-band antenna, the measured results are in agreement with the simulated ones, showing a decrease in the magnitude of the return loss in the resonance frequencies, with the main factors being attributed to the realistic conditions (lossy environment different from the simulated one) and the influence of the RF cable connected to the antenna, that introduces current leakage and electromagnetic scattering. Nevertheless, the resonance frequencies were not affected, and so the outcome is a dual-band antenna that works in the ISM operating bands of 2.45 and 5.8 GHz, and is proven robust against the effect of the electromagnetic properties of the human tissues. Thus, it is suitable for WBAN applications.

Regarding the UWB antenna, the results measured in a free-space scenario indicate that the antenna only covers the standard UWB frequency range only if the $-6dB$ is accepted. The influence of the RF cable is seen to be of great influence to the performance of the antenna, and the precision of the fabrication of it must also be taken into account, since the antenna is much smaller than the dual-band one and thus requires a certain level of rigour in its manufacturing. In terms of measurements with the antenna on the human user, the results show again a severe impact on the operation band of the UWB antenna. It is seen that the lower frequencies suffer an up-shift of around 2 GHz and a decrease on their magnitudes, and there is even a small range of frequencies in which the return loss is higher than $-6dB$. However, the higher frequencies are not as much affected, pointing out one of the properties of the CPW solution. Also, the results are accordant to the expected ones; the lack of a copper shielding on the back not only allows for a low front-to-back ratio (which is not desirable for antennas that are meant to be used in the proximity of a human body), but also an inefficient way of improving on and off-body communications. It is seen the sensitivity of the CPW solution to the same influence, and thus a microstrip solution could be in order.

Finally, the author believes the current dissertation has met all of the proposed goals, and gave a small contribution to the world of wireless area networks. The antennas are the heart of those communication systems, and must be developed with precision in order to allow the communication between devices the best possible way and deliver the best quality of service to the targeted users.

5.2 Future Work

This dissertation has provided a dual-band antenna that is robust against the electromagnetic influence of human body tissues. As a simpler project, and still regarding not flexible materials, the antenna can be further optimized in terms of the materials used for its construction. Materials with higher permittivity can be used, as an attempt to reduce the physical dimensions of the antenna, such as the $RogersRO3200$. Also, regarding the fabrication process, a different fabrication method should be employed, in order to approximate the measured results from the simulated ones. To keep the project cost-effective, perhaps the inkjet printing is one of the fabrication methods to consider. Furthermore, the antenna can be tested in different scenarios, according to its envisioned application. It can be subjected to different climate changes, whether is the range of temperatures in which the antenna still functions

properly; verify the resistance of the antenna to water; figure out the amount of force the antenna can handle before it breaks or starts losing its properties.

For more ambitious works, the narrow-bands of the dual-band antenna are interesting for Internet of Things (IoT) applications. The dual frequency property of the designed microstrip patch antenna presents an opportunity to study the double system capacity by frequency reuse. The antenna can be regulated to a certain polarization diversity in order to improve the reception and transmission performance. Nowadays, the need for smaller devices is of great importance, but that space saving can also be translated into having a reconfigurable antenna which, although it is just one, can provide for multiple systems.

Another application for this antenna is to integrate it in a PCB, which together with a battery can produce a geolocation device. With small alterations on the design of the antenna, one can perform a down-shift on the resonance frequencies, so to fix one at 1.57 GHz and cover the GPS band.

Regarding medical and military applications, the antenna can be easily integrated into a device that collects physiological data and measures the vital signs of a patient/soldier, communicates them to the antenna, which will retransmit them to an off-body device that is monitored by someone. In case of communication failure, it is one way of ensuring they get help as fast as possible, as it allows doctors to obtain real-time access to health data. The dual-band property may use a frequency for transmitting and the other to receive, or employ a full duplex mode and allow for redundancy, in case one of the frequencies gets blocked or suffers severe interference from other bands.

As for the UWB antenna, it can be further optimized in order to respect the $-10dB$ criteria for the whole UWB standard frequency range. Other materials for the substrate can be used, in order to improve the return loss and to continue to diminish the physical dimensions of the antenna. Also, the GCPW solution was not fully expanded, but the combination of the microstrip and the CPW properties is very attractive and should therefore be deepened for this antenna. The use of a copper shield is a characteristic that should be studied in a more insightful way, in order to build a electromagnetic influence-free antenna. Nevertheless, an optimization of the UWB antenna is in order, and the CPW solution should be reviewed, as it allows for an easy integration with active devices. An example of it is to connect the antenna into a device that can reconfigure its output parameters (radiation pattern, directivity and more) according to the changing environment, and thus enhance the properties of the UWB antenna.

Appendix A

SMA Connector

Since an antenna can not be physically measured without something to guide the electromagnetic waves, the SMA connector from Farnell components from Figure A.1(a) was used [14]. In order to account for the influence of the connector on the performance of the antennas, a simulated model of the same connector was included in the $CSTMicrowaveStudio$ software. This model was provided by Professor António Alves Moreira.

(a) SMA connector, by Farnell [14].

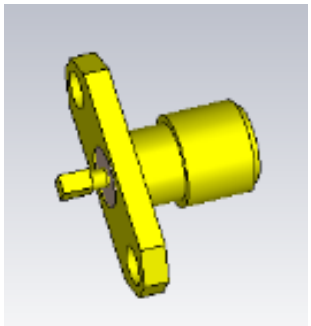

(b) SMA connector used for simulation purposes.

Figure A.1: SMA connectors employed for measuring the antennas.

Appendix B

AutoCAD Masks

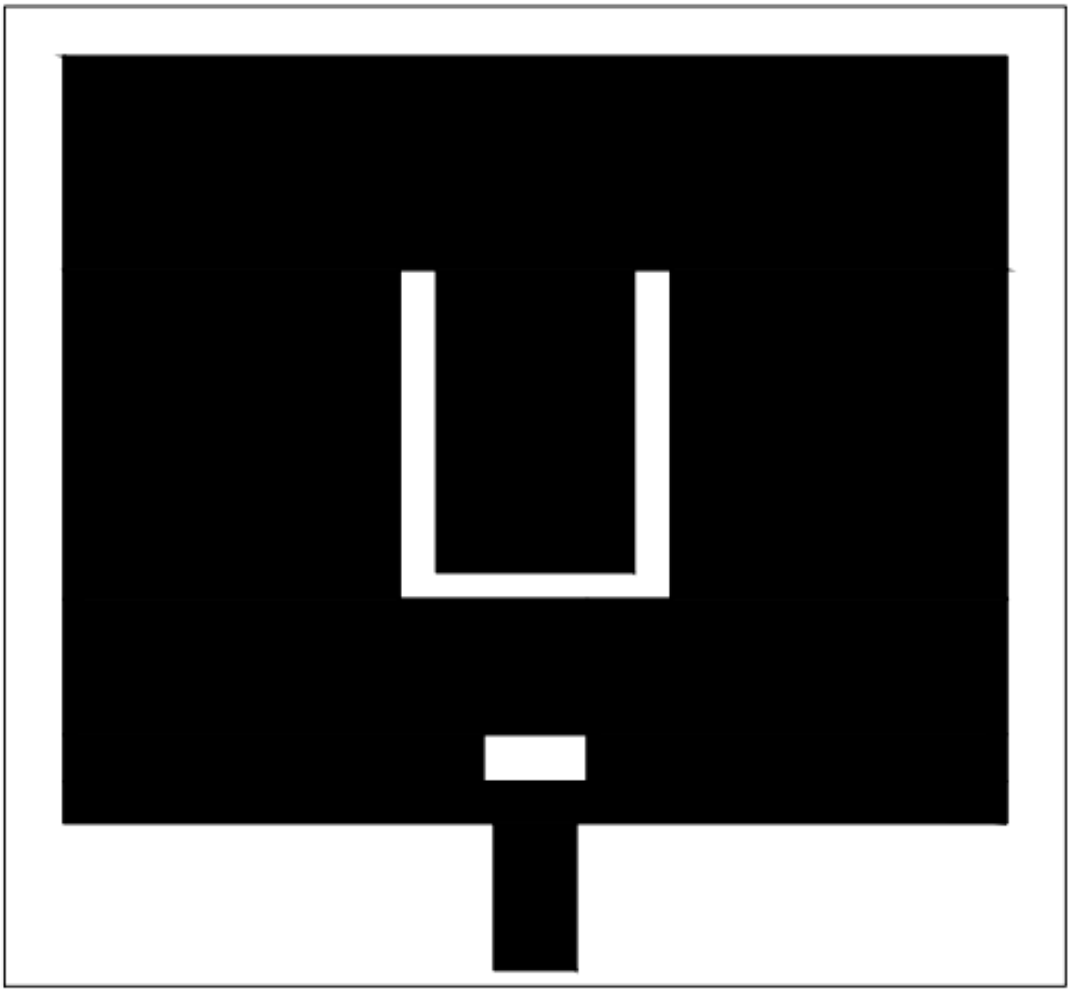

Figure B.1: AutoCAD mask used to produce the proposed microstrip dual-band patch antenna.

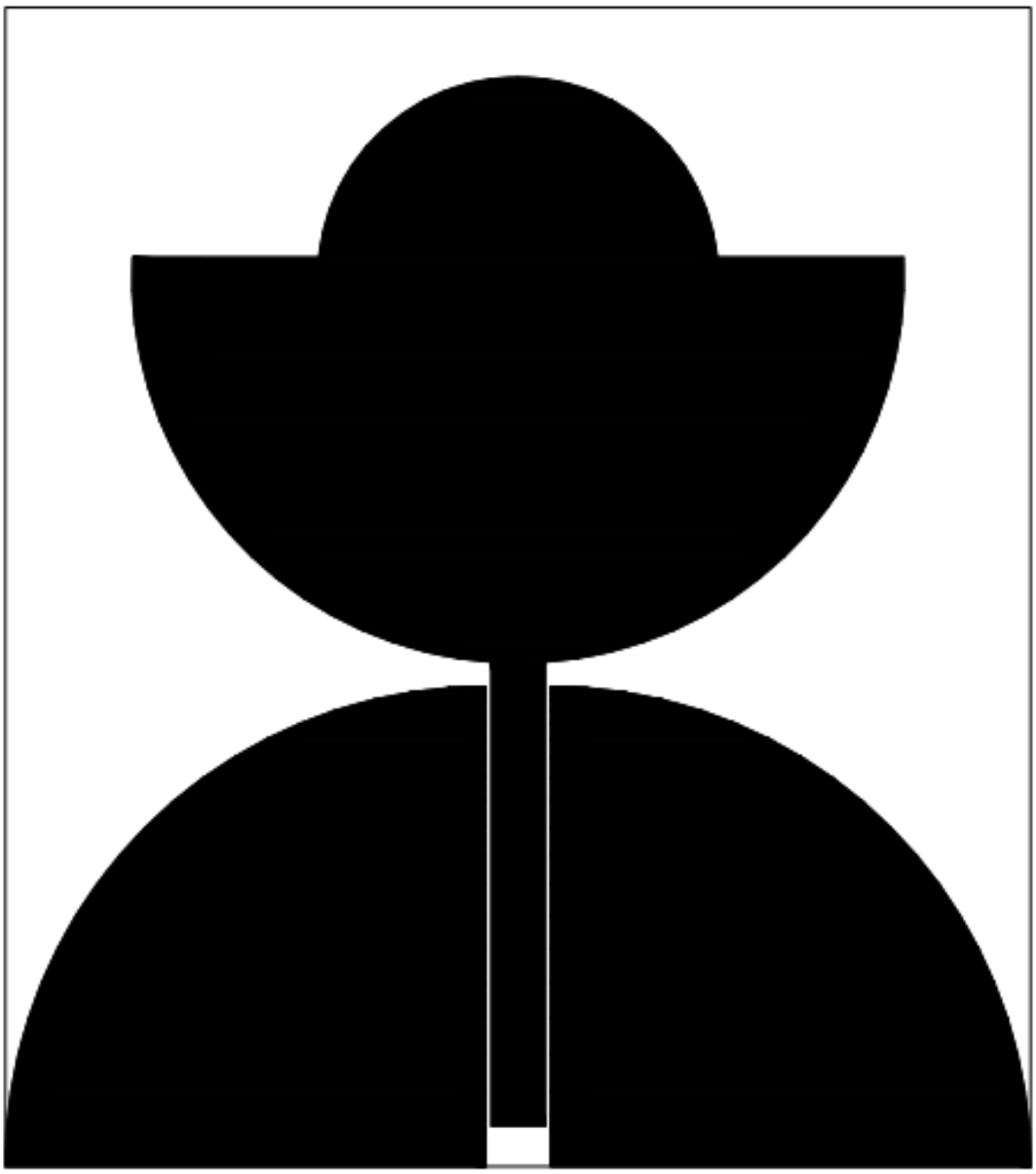

Figure B.2: AutoCAD mask used to produce the proposed CPW-fed UWB antenna.

Bibliography

[1] Comparing microstrip and grounded coplanar waveguide. Technical report, Microwave Journal, May 2015. URL http://www.microwavejournal.com/blogs/1-rog-blog/post/24374-comparing-microstrip-and-grounded-coplanar-waveguide.

[2] D. Abed and H. Kimouche. *Design and characterization of microstrip UWB antennas*. INTECH Open Access Publisher, 2010.

[3] M. Al-Husseini, A. Ramadan, Y. Tawk, A. El-Hajj, and K. Y. Kabalan. Design and ground plane optimization of a cpw-fed ultra-wideband antenna. *Turkish Journal of Electrical Engineering & Computer Sciences*, 19(2):243–250, 2011.

[4] Y. Al-Naiemy, T. A. Elwi, H. R. Khaleel, and H. Al-Rizzo. A systematic approach for the design, fabrication, and testing of microstrip antennas using inkjet printing technology. *ISRN Communications and Networking*, 2012:5, 2012.

[5] A. Alomainy, Y. Hao, and F. Pasveer. Numerical and experimental evaluation of a compact sensor antenna for healthcare devices. *Biomedical Circuits and Systems, IEEE Transactions on*, 1(4): 242–249, Dec 2007. ISSN 1932-4545. doi: 10.1109/TBCAS.2007.913127.

[6] J. ao Manuel Coelho Vicente. Projecto e estudo de antenas em tecido para aplicação em vestuário. Master's thesis, Instituto Superior Técnico (IST), June 2010.

[7] J. ao Vicente Faria. Flexible antennas design and test for human body applications scenarios. Master's thesis, Instituto Superior Técnico (IST), May 2015.

[8] Q. Bai and R. Langley. Bending of a small coplanar textile antenna. In *Antennas and Propagation Conference (LAPC), 2010 Loughborough*, pages 329–332, Nov 2010. doi: 10.1109/LAPC.2010.5666263.

[9] M. Bevan. Electromagnetic analysis of horn antennas in the terahertz region. Master's thesis, NUI Maynooth, Ireland, May 2013.

[10] P. J. Bevelacqua. Antenna theory, 2009. URL http://www.antenna-theory.com/.

[11] N. Chahat, M. Zhadobov, R. Sauleau, and K. Ito. A compact uwb antenna for on-body applications. *IEEE Transactions on Antennas and Propagation*, 59(4):1123–1131, April 2011. ISSN 0018-926X. doi: 10.1109/TAP.2011.2109361.

[12] J. Coonrod and B. Rautio. Comparing microstrip and cpw performance. *Microwave Journal*, 55(7): 74–86, 2012.

[13] A. Elrashidi, K. Elleithy, and H. Bajwa. The fringing field and resonance frequency of cylindrical microstrip printed antenna as a function of curvature. *International Journal of Wireless Communications and Networking (IJWCN)*, 2011.

[14] Farnell. Sma connectors. URL `http://www.te.com/usa-en/product-1-1478963-0.html`.

[15] FOTOFAB. The chemical etching process. URL `http://www.fotofab.com/chemical-etching-process.php`.

[16] I. Foundation. Virtual family: Whole-body human models. URL `http://www.itis.ethz.ch/index/index_humanmodels.html`.

[17] P. S. Hall and Y. Hao. *Antennas and Propagation for Body-Centric Wireless Communications. Second Edition*. Artech House, Inc., Norwood, MA, USA, 2nd edition, 2012. ISBN 1608073769, 9781608073764.

[18] W. Hirt. The european uwb radio regulatory and standards framework: Overview and implications. In *2007 IEEE International Conference on Ultra-Wideband*, pages 733–738, Sept 2007. doi: 10.1109/ICUWB.2007.4381041.

[19] C. Hung and T. Chiu. Dual-band reconfigurable antenna design using slot-line with branch edge. *IEEE Transactions on Antennas and Propagation*, 63(2):508–516, Feb 2015. ISSN 0018-926X. doi: 10.1109/TAP.2014.2382121.

[20] ICNIRP. Guidelines for limiting exposure to time-varying electric, magnetic, and electromagnetic fields, up to 300 ghz. URL `http://www.icnirp.org/cms/upload/publications/ICNIRPemfgdl.pdf`.

[21] IFAC-CNR. Dielectric properties of body tissues. URL `http://niremf.ifac.cnr.it/tissprop/`.

[22] K. Ito and N. Haga. Basic characteristics of wearable antennas for body-centric wireless communications. In *Antennas and Propagation Conference (LAPC), 2010 Loughborough*, pages 42–47, Nov 2010. doi: 10.1109/LAPC.2010.5666804.

[23] K. Ito and H. Kawai. Solid phantoms for evaluation of interactions between the human body and antennas. In *IWAT 2005. IEEE International Workshop on Antenna Technology: Small Antennas and Novel Metamaterials, 2005.*, pages 41–44, March 2005. doi: 10.1109/IWAT.2005.1460993.

[24] I. T. U. (ITU). *Radio Regulations: Articles*. 2012. ISBN 978-92-61-14021-2. URL `http://www.itu.int/dms_pub/itu-s/oth/02/02/S02020000244501PDFE.PDF`.

[25] . Januszkiewicz and S. Hausman. Simplified human phantoms for wireless body area network modelling. In *2015 9th European Conference on Antennas and Propagation (EuCAP)*, pages 1–4, May 2015.

[26] N. M. Jizat, S. K. A. Rahim, Y. C. Lo, and M. M. Mansor. Compact size of cpw dual-band meander-line transparent antenna for wlan applications. In *Applied Electromagnetics (APACE), 2014 IEEE Asia-Pacific Conference on*, pages 20–22, Dec 2014. doi: 10.1109/APACE.2014.7043779.

[27] H. R. Khaleel, A. I. Abbosh, and H. M. Al-Rizzo. *Design, fabrication, and testing of flexible antennas*. INTECH Open Access Publisher, 2013.

[28] M. T. Koichi Ito and K. Saito. Small antennas used in the vicinity of human body. *IEICE Transactions*, 99-B(1):9–18, 2016. URL `http://search.ieice.org/bin/summary.php?id=e99-b_1_9`.

[29] M. Koohestani. *Human Body Proximity Effects on Ultra-Wideband Antennas*. PhD thesis, École Polytechnique Fédérale de Lausanne and Instituto Superior Técnico, September 2014.

[30] M. Koohestani, N. Pires, A. K. Skrivervik, and A. A. Moreira. Influence of the human body on a new coplanar-fed ultra-wideband antenna. In *2012 6th European Conference on Antennas and Propagation (EUCAP)*, pages 316–319, March 2012. doi: 10.1109/EuCAP.2012.6205976.

[31] K. P. Kumar, K. S. Rao, V. M. Rao, K. Uma, A. Somasekhar, and C. M. Mohan. The effect of dielectric permittivity on radiation characteristics of co-axially feed rectangular patch antenna: Design & analysis. *International journal of Advanced Research in Computer and communication Engineering*, 2(2):1254–1258, 2013.

[32] R. Kumar, J. Shinde, and M. Uplane. Effect of slots in ground plane and patch on microstrip antenna performance. *International Journal of Recent Trends in Engineering*, 2(6):34–36, 2009.

[33] K. S. Kwak, S. Ullah, and N. Ullah. An overview of ieee 802.15.6 standard. In *2010 3rd International Symposium on Applied Sciences in Biomedical and Communication Technologies (ISABEL 2010)*, pages 1–6, Nov 2010. doi: 10.1109/ISABEL.2010.5702867.

[34] K. F. Lee, S. L. S. Yang, and A. A. Kishk. U-slot patch antennas for dual-band or multi-band applications. In *Antenna Technology, 2009. iWAT 2009. IEEE International Workshop on*, pages 1–4, March 2009. doi: 10.1109/IWAT.2009.4906900.

[35] K. F. Lee, K. M. Luk, T. Mak, and S. Yang. Dual and triple band stacked patch antennas with u-slots. In *Proceedings of the Fourth European Conference on Antennas and Propagation*, pages 1–5, April 2010.

[36] K. F. Lee, K. M. Luk, K. M. Mak, and S. L. S. Yang. On the use of u-slots in the design of dual-and triple-band patch antennas. *IEEE Antennas and Propagation Magazine*, 53(3):60–74, June 2011. ISSN 1045-9243. doi: 10.1109/MAP.2011.6028422.

[37] K.-S. Lim, M. Nagalingam, and C.-P. Tan. Design and construction of microstrip uwb antenna with time domain analysis. *Progress In Electromagnetics Research M*, 3:153–164, 2008.

[38] M. A. Malek, S. Hakimi, S. K. A. Rahim, and A. K. Evizal. Dual-band cpw-fed transparent antenna for active rfid tags. *IEEE Antennas and Wireless Propagation Letters*, 14:919–922, 2015. ISSN 1536-1225. doi: 10.1109/LAWP.2014.2387157.

[39] N. T. Markad, R. D. Kanphade, and D. G. Wakade. Design of cavity model microstrip patch antenna. 6(4), 2015. ISSN 2222-1719 (Paper) ISSN 2222-2863 (Online).

[40] J. M. D. C. Mesquita. Ism flexible dual-band antenna. Master's thesis, Instituto Superior Técnico (IST), October 2012.

[41] S. Mishra and O. S. Hada. Broadband microstrip patch antenna using slot. *International Journal of Computer Applications*, 108(6), 2014.

[42] A. T. Mobashsher and A. M. Abbosh. Artificial human phantoms: Human proxy in testing microwave apparatuses that have electromagnetic interaction with the human body. *IEEE Microwave Magazine*, 16(6):42–62, July 2015. ISSN 1527-3342. doi: 10.1109/MMM.2015.2419772.

[43] W. C. Mok, S. H. Wong, K. M. Luk, and K. F. Lee. Single-layer single-patch dual-band and triple-band patch antennas. *IEEE Transactions on Antennas and Propagation*, 61(8):4341–4344, Aug 2013. ISSN 0018-926X. doi: 10.1109/TAP.2013.2260516.

[44] A. M. R. G. A. Moreira. *Antenas Impressas*. Instituto Superior Técnico (IST).

[45] S. Movassaghi, M. Abolhasan, J. Lipman, D. Smith, and A. Jamalipour. Wireless body area networks: A survey. *Communications Surveys Tutorials, IEEE*, 16(3):1658–1686, Third 2014. ISSN 1553-877X. doi: 10.1109/SURV.2013.121313.00064.

[46] W. Nakamura and T. Maeda. The effects of feeding cable arrangements on radiation pattern measurements using scale model phantoms. In *Antenna Technology: Small Antennas and Novel Metamaterials, 2008. iWAT 2008. International Workshop on*, pages 350–353, March 2008. doi: 10.1109/IWAT.2008.4511352.

[47] P. Nepa and G. Manara. Design and characterization of wearable antennas. In *Electromagnetics in Advanced Applications (ICEAA), 2013 International Conference on*, pages 1168–1171, Sept 2013. doi: 10.1109/ICEAA.2013.6632428.

[48] C. Oliveira, C. Lopes, M. Mackowiak, and L. M. Correia. Characterisation of on-body communications at 2.45 ghz. In *Proceedings of the 6th International Conference on Body Area Networks*, BodyNets '11, pages 54–59, ICST, Brussels, Belgium, Belgium, 2011. ICST (Institute for Computer Sciences, Social-Informatics and Telecommunications Engineering). ISBN 978-1-936968-29-9. URL `http://dl.acm.org/citation.cfm?id=2318776.2318790`.

[49] D. Orban and G. Moernaut. The basics of patch antennas, updated. *RF Globalnet Newsletter*, September 2009.

[50] Y. Ouyang and W. J. Chappell. High frequency properties of electro-textiles for wearable antenna applications. *IEEE Transactions on Antennas and Propagation*, 56(2):381–389, Feb 2008. ISSN 0018-926X. doi: 10.1109/TAP.2007.915435.

[51] D. L. Paul, H. Giddens, M. G. Paterson, G. S. Hilton, and J. P. McGeehan. Impact of body and clothing on a wearable textile dual band antenna at digital television and wireless communications bands. *IEEE Transactions on Antennas and Propagation*, 61(4):2188–2194, April 2013. ISSN 0018-926X. doi: 10.1109/TAP.2012.2232632.

[52] J. Pinto, L. Tween, B. Henderson, and R. Lewis. Vox, video and data sharing using body worn antennas. In *Antennas and Propagation Conference (LAPC), 2011 Loughborough*, pages 1–4, Nov 2011. doi: 10.1109/LAPC.2011.6114123.

[53] Priyanka, A. Kumar, and R. Arora. Effect of slot rotation on rectangular slot based microstrip patch antenna. *International Journal of Current Engineering and Technology*, 5(4):2322–2327, August 2015.

[54] P. Puttaswamy, P. S. K. Murthy, and B. A. Thomas. Analysis of loss tangent effect on microstrip antenna gain. *Int. Journal of Applied Sciences and Engineering Research*, 3:1102–1107, November 2014.

[55] M. Rani, A. Tharek, T. Peter, S. Cheung, and S. Rahim. Dual-band transparent antenna for ism band applications. 2013. URL `http://hdl.handle.net/10722/189917`.

[56] B. R. Rao, W. Kunysz, R. Fante, and K. McDonald. *GPS/GNSS Antennas*. Artech House, 2013.

[57] J. Roças, N. Pires, and A. A. Moreira. Human body effects on the matching of a 2.45 ghz coplanar-fed antenna. In *Antennas and Propagation (EuCAP), 2013 7th European Conference on*, pages 3279–3281, April 2013.

[58] J. F. S. Roças. Projeto de uma antena para utilização junto ao corpo humano. Master's thesis, Instituto Superior Técnico (IST), October 2012.

[59] *RT/Duroid 5880*. Rogers Corporation, 100 S. Roosevelt Avenue, Chandler, AZ 85226 U.S.A. URL `http://www.rogers-corp.com/mwu/`.

[60] I. Rosu. Microstrip, stripline, and cpw design. *Available: in http://www. qsl. net/va3iul*, 2013.

[61] B. Sanz-Izquierdo and J. Batchelor. A dual band belt antenna. In *Antenna Technology: Small Antennas and Novel Metamaterials, 2008. iWAT 2008. International Workshop on*, pages 374–377, March 2008. doi: 10.1109/IWAT.2008.4511358.

[62] B. Sanz-Izquierdo, F. Huang, and J. C. Batchelor. Small size wearable button antenna. In *2006 First European Conference on Antennas and Propagation*, pages 1–4, Nov 2006. doi: 10.1109/EUCAP.2006.4584568.

[63] A. Tsolis, W. G. Whittow, A. A. Alexandridis, and J. C. Vardaxoglou. Evaluation of a human body phantom for wearable antenna measurements at the 5.8ghz band. In *Antennas and Propagation Conference (LAPC), 2013 Loughborough*, pages 414–419, Nov 2013. doi: 10.1109/LAPC.2013.6711932.

[64] M. Ur-Rehman, Q. H. Abbasi, X. Chen, and Z. Ying. Numerical modelling of human body for bluetooth body-worn applications. *Progress in Electromagnetics Research*, 143:623–629, 2013.

[65] J. Vicente and A. Moreira. Electro-textile printed slot antenna over finite ebg structure. In *Antenna Technology (iWAT), 2010 International Workshop on*, pages 1–4, March 2010. doi: 10.1109/IWAT.2010.5464688.

[66] C.-H. Wu, K.-L. Wong, Y.-C. Lin, and S.-W. Su. Conformal bluetooth antenna for the watch-type wireless communication device application. In *2007 IEEE Antennas and Propagation Society International Symposium*, pages 4156–4159, June 2007. doi: 10.1109/APS.2007.4396456.

[67] B. Yeboah-Akowuah, P. Kosmas, and Y. Chen. A low profile microstrip patch antenna for body-centric communications at 2.45ghz band. In *Antennas and Propagation (EuCAP), 2015 9th European Conference on*, pages 1–3, April 2015.

[68] K. B. Yi Huang. *Antennas: From Theory to Practice*, chapter 5, pages 184–191. John Wiley and Sons, Ltd, 2008. ISBN: 978-0-470-51028-5.

[69] K. Zhao, Z. Ying, and S. He. Antenna designs of smart watch for cellular communications by using metal belt. In *Antennas and Propagation (EuCAP), 2015 9th European Conference on*, pages 1–5, April 2015.